Supplemental material to this article can be found at:
http://molpharm.aspetjournals.org/content/suppl/2021/05/24/molpharm.120.000184.DC1
1521-0111/100/2/155–169$35.00 https://doi.org/10.1124/molpharm.120.000184
MOLECULAR PHARMACOLOGY Mol Pharmacol 100:155–169, August 2021

Cysteine Modification by Ebselen Reduces the Stability and Cellular Levels of 14-3-3 Proteins

Kai Waløen, Kunwar Jung-KC, Elisa D. Vecchia, Sunil Pandey, Norbert Gasparik, Anne Døskeland, Sudarshan Patil, Rune Kleppe, Jozef Hritz, William H.J. Norton, Aurora Martinez, and Jan Haavik

Department of Biomedicine (K.W., K.J.K.C., S.Pan., A.D., S.Pat., A.M., J.Ha.), Proteomics Unit (PROBE), (A.D.), University of Bergen, Bergen, Norway; Department of Neuroscience, Psychology and Behaviour, College of Medicine, Biological Sciences and Psychology, University of Leicester, Leicester, UK (E.D.V., W.H.J.N.); CEITEC-MU, Masaryk University, Brno, Czech Republic (N.G., J.Hr.); Department of Chemistry, Faculty of Science, Masaryk University, Brno, Czech Republic and Norwegian Centre for Maritime and Diving Medicine, Department of Occupational Medicine (R.K.), Division of Psychiatry (J.Ha.), Haukeland University Hospital, Bergen, Norway

Received November 16, 2020; accepted May 11, 2021

ABSTRACT

The 14-3-3 proteins constitute a family of adaptor proteins with many binding partners and biological functions, and they are considered promising drug targets in cancer and neuropsychiatry. By screening 1280 small-molecule drugs using differential scanning fluorimetry (DSF), we found 15 compounds that decreased the thermal stability of 14-3-3ζ. Among these compounds, ebselen was identified as a covalent, destabilizing ligand of 14-3-3 isoforms ζ, ε, γ, and η. Ebselen bonding decreased 14-3-3ζ binding to its partner Ser19-phosphorylated tyrosine hydroxylase. Characterization of site-directed mutants at cysteine residues in 14-3-3ζ (C25, C94, and C189) by DSF and mass spectroscopy revealed covalent modification by ebselen of all cysteines through a selenylsulfide bond. C25 appeared to be the preferential site of ebselen interaction in vitro, whereas modification of C94 was the main determinant for protein destabilization. At therapeutically relevant concentrations, ebselen and ebselen oxide caused decreased 14-3-3 levels in SH-SY5Y cells, accompanied with an increased degradation, most probably by the ubiquitin-dependent proteasome pathway. Moreover, ebselen-treated zebrafish displayed decreased brain 14-3-3 content, a freezing phenotype, and reduced mobility, resembling the effects of lithium, consistent with its proposed action as a safer lithium-mimetic drug. Ebselen has recently emerged as a promising drug candidate in several medical areas, such as cancer, neuropsychiatric disorders, and infectious diseases, including coronavirus disease 2019. Its pleiotropic actions are attributed to antioxidant effects and formation of selenosulfides with critical cysteine residues in proteins. Our work indicates that a destabilization of 14-3-3 may affect the protein interaction networks of this protein family, contributing to the therapeutic potential of ebselen.

SIGNIFICANCE STATEMENT

There is currently great interest in the repurposing of established drugs for new indications and therapeutic targets. This study shows that ebselen, which is a promising drug candidate against cancer, bipolar disorder, and the viral infection coronavirus disease 2019, covalently bonds to cysteine residues in 14-3-3 adaptor proteins, triggering destabilization and increased degradation in cells and intact brain tissue when used in therapeutic concentrations, potentially explaining the behavioral, anti-inflammatory, and antineoplastic effects of this drug.

Introduction

The 14-3-3 proteins constitute a family of highly conserved acidic proteins that form homo- and heterodimers between isoforms. The seven human isoforms of 14-3-3 (β, ε, η, γ, θ, σ, and ζ) are encoded by different genes (Aitken 2006; Yang et al., 2006). Although 14-3-3 proteins have no enzymatic activity, their binding to phosphorylated partners exerts chaperone as well as regulatory functions (van Heusden, 2005). As such, 14-3-3 proteins are involved in many vital cellular functions, such as transcription, intracellular trafficking, cytoskeletal structure, metabolic regulation, and apoptosis (Aitken, 2006; Obsil and Obsilova, 2011).

Dimers of 14-3-3 protein present an overall W-shaped structure, with the ligand binding grooves facing each other. Each subunit has a characteristic C shape and is made up of nine antiparallel α-helices (Fig. 1A). The canonical binding site for protein-protein interaction (PPI) in 14-3-3 is situated

This work has received funding from the European Union's Horizon 2020 research and innovation program [Marie Sklodowska-Curie Grant Agreement 643051], European Union's Horizon 2020 research and innovation program [Grant Agreement 667302] (Comorbid Conditions of ADHD; CoCA), Stiftelsen Kristian Gerhard Jebsen [SKJ-MED-02], The Regional Health Authority of Western Norway [25048] (to J.Ha.) and [912246] (to A.M., NevSom (Grant 18/09147), the Research Council of Norway (RCN) [Grant FRIMEDBIO 261826/F20] (to A.M.), and the infrastructure projects Nor-Openscreen (RCN) [245922/F50] and EU-Openscreen (to A.M.). J.Hr. and N.G. acknowledge funding from the Czech Science Foundation [GF20-05789L] and European Regional Development Fund-Project CIISB4HEALTH [CZ.02.1.01/0.0/0.0/16_013/0001776], which also partially supported the measurements at the Proteomics Core Facility, Central European Institute of Technology - Masaryk University. A.D. acknowledges that LC-MS/MS was carried out at the Proteomics Unit (PROBE), University of Bergen.

Funding support for this article was provided by the NevSom (18/09147).

J.Ha. has received speaker honoraria from Lilly, Shire, HB Pharma, Medice, Takeda, and Biocodex. The authors declare no other conflicts of interest.

dx.doi.org/10.1124/molpharm.120.000184.

on the concave surface of each subunit, and binding of a partner protein to 14-3-3 proteins is typically dependent on a phosphorylated Ser or Thr flanked by Arg and Pro residues (Aitken, 2006; Obsil and Obsilova, 2011).

The 14-3-3 proteins regulate many cellular processes involved in cancer and neuropsychiatric and metabolic disorders (Hermeking, 2003; Pennington et al., 2018; Diallo et al., 2019; Torrico et al., 2020). Overall, 14-3-3 proteins have >2000 predicted binding partners, and >200 of these have been experimentally identified (Hermeking, 2003; Pozuelo Rubio et al., 2004; Aitken, 2006; Xiao et al., 2014; Pagan et al., 2017; Ballone et al., 2018). PPIs are considered a promising field in drug discovery. It has been shown that peptides and derivatives, small-molecule compounds, and natural products can modulate these PPIs (Stevers et al., 2018). In this context, 14-3-3 proteins are interesting targets because of their large number of binding partners with therapeutic relevance. There are several natural and synthetic stabilizers of 14-3-3 PPIs, such as fusicoccin, cotylenin A, and mizoribine, which originate from fungus, as well as semisynthetic fusicoccin derivatives (Ballone et al., 2018) and synthetic stabilizers, including molecular tweezers (Bier et al., 2016). On the other hand, some peptides and small-molecule compounds, such as R18 and BV02, may function as disruptors of 14-3-3 PPIs (Ballone et al., 2018). 14-3-3 function also seems to be regulated by oxidation of critical cysteine residues, suggesting additional potential sites for pharmacological intervention (Kim et al., 2014).

Here, we report the characterization of a previously unobserved effect of ebselen on 14-3-3 proteins at the molecular, cellular, and animal levels. These effects are associated with a covalent interaction with 14-3-3 cysteine residues. Ebselen can interact covalently with cysteine residues in several protein targets (Favrot et al., 2013; Joice et al., 2013; Lieberman et al., 2014; Mukherjee et al., 2014). It seems to bind to all 14 Cys residues of the nonstructural protein 3 helicase (Mukherjee et al., 2014), but it has also been reported to only interact with specific Cys residues in, e.g., superoxide dismutase 1 (Capper et al., 2018). Modification of Cys residues by ebselen has been reported to inhibit enzymatic function by forcing conformational changes in target proteins (Favrot et al., 2013; Mukherjee et al., 2014). Ebselen has been proposed as a safe lithium mimetic (Singh et al., 2013, 2016; Masaki et al., 2016) and has been subject to phase II clinical trials for bipolar disorder. Ebselen is also in clinical trials for hearing disorders, diabetes, and COVID-19 (https://clinicaltrials.gov/). Out of 10,000 approved drugs and compounds in clinical trials, ebselen showed the strongest inhibition of the main protease (M^{pro}) of SARS-CoV-2 (Jin et al., 2020). Ebselen has also shown activity against other virus protein targets and has been proposed to protect against organ injury caused by COVID-19 (Menendez et al., 2020; Sies and Parnham, 2020). Here, we show that although all Cys residues in 14-3-3 proteins have the potential to be modified by ebselen, they have different reactivities, and a single residue (C94) is responsible for the protein destabilization observed at low concentrations of ebselen. Ebselen is capable of crossing the blood-brain barrier and is pharmacologically active in the brain, making it a compound of interest in drug discovery campaigns related to neurological disorders (Singh et al., 2013). We propose that our findings may provide a foundation for further studies on the repurposing of ebselen and its use as a covalent modulator of 14-3-3 PPI with several therapeutic implications.

Materials and Methods

Materials

The Prestwick Chemical Library from Prestwick Chemical (purchased in 2014) was used for screening. This library consists of 1280 small molecules, of which 95% are approved drugs, at a concentration of 10 mM in 100% DMSO. Ebselen and ebselen oxide were ordered from Sigma-Aldrich (E3520; 2018), except for the experiments in zebrafish, for which it was ordered from Cayman Chemical (70530; 2018). Active p38-regulated/activated protein kinase (PRAK) was from University of Dundee, Medical Research Council Protein Phosphorylation and Ubiquitylation Unit Reagents and Services. [^{32}P-γ]ATP was from PerkinElmer (GA). Shrimp alkaline phosphatase was from New England Biolabs.

Protein Expression, Purification, and Preparation of Ebselen-Treated 14-3-3ζ

Glutathione *S*-transferase–tagged 14-3-3ζ was expressed in *Escherichia coli* (BL21- CodonPlusDE3; Agilent Technologies) (Kleppe et al., 2014). The cells were lysed using a French press in PBS buffer (pH 7.4). The glutathione *S*-transferase–tagged 14-3-3ζ was immobilized on Glutathione Sepharose 4B (GE Healthcare) and cleaved overnight at 4°C using 10 U/mL of thrombin (Sigma-Aldrich). The cleaved 14-3-3ζ was collected as flow through. The flow through was filtered using Ultrafree-MC GV centrifugation filters (Merck) and purified further on a Superdex 200 increase 10/300 GL (GE Healthcare) gel filtration column using 20 mM HEPES and 200 mM NaCl (pH 7.4). The 14-3-3ζ peak was collected and concentrated using Amicon Ultra 15-ml Centrifugal Filters with a cutoff of 30,000 Da (Merck). 14-3-3γ, η, and ε were purified as previously reported (Kleppe et al., 2014; Ghorbani et al., 2016). 14-3-3 cysteine mutants were prepared as previously reported (Jandova et al., 2018). TH expression, purification, and phosphorylation were performed as reported (Kleppe et al., 2014). Dephosphorylation assay was performed in 15 mM HEPES, 150 mM NaCl (pH 7.4), and 10% glycerol, using TH labeled on Ser19 by PRAK and shrimp alkaline phosphatase essentially as described (Kleppe et al., 2014; Ghorbani et al., 2016), except that no reducing agents were used. Thus, TH (2 mg/ml) was phosphorylated using active PRAK (7 U/ml) essentially as described (Kleppe et al., 2014; Ghorbani et al., 2016), but in 15 mM HEPES (pH 7.4), 150 mM NaCl, and 10% glycerol without reducing agents, and the PRAK inhibitor epigallocatechin gallate was added (100 μM) after 30 minutes (25°C) and pSer19TH was kept on ice until used for dephosphorylation. TH (2 μM) with or without 14-3-3 (10 μM) was preincubated on ice for 5 minutes before starting the dephosphorylation reaction (25°C) by adding shrimp alkaline phosphatase (0.12 U/μl) and the remaining ^{32}P-labeled TH was sampled on phosphocellulose filters washed in phosphoric acid. Dephosphorylation sample without added phosphatase showed stable levels of

ABBREVIATIONS: CD, circular dichroism; CID, collision-induced dissociation; COVID-19, coronavirus disease 2019; DAPI, diamidino-2-phenylindole; DSF, differential scanning fluorimetry; GAPDH, glyceraldehyde-3-phosphate dehydrogenase; MALDI, matrix-assisted laser desorption/ionization; MS, mass spectroscopy; MS/MS, tandem mass spectrometry; PDB, Protein Data Bank; PPI, protein-protein interaction; PRAK, p38-regulated/activated protein kinase; pSer19TH, Ser19-phosphorylated TH; PVDF, polyvinylidene difluoride; RRID, Research Resource Identifiers; SPR, surface plasmon resonance; TH, tyrosine hydroxylase; TOF, time of flight; TPH, tryptophan hydroxylase; WT, wild-type; Z-VAD-FMK, Benzyloxycarbonyl-Val- Ala-Asp(OMe)-fluoromethylketone.

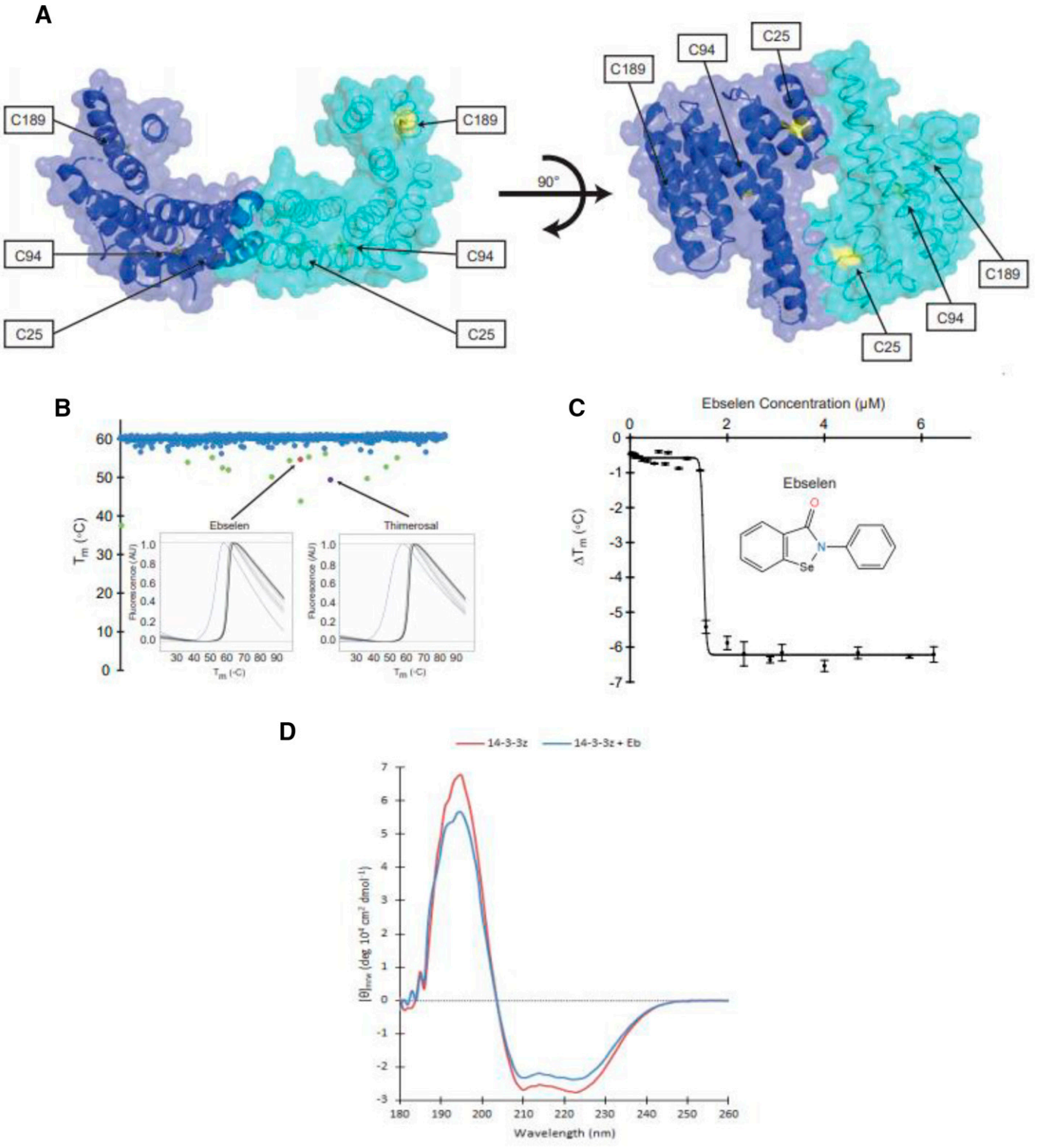

Fig. 1. Screening of drugs interacting with 14-3-3ζ, and the destabilization caused by ebselen. (A) The three-dimensional structure of dimeric 14-3-3ζ (PDB: 1A4O) in ribbon and transparent surface representation. Cysteine residues are colored yellow. C25 and C189 are surface-accessible, and C94 is embedded within the protein. (B) DSF-based screening of 14-3-3ζ with the Prestwick Chemical Library (1280 compounds). All T_m values obtained are represented; blue dots indicate the compounds that provide a T_m value for 14-3-3ζ within 10 × S.D. of the 4% DMSO control (T_m = 61.1 ± 0.5°C), and green dots indicate primary hits, all causing a decrease in the T_m of 14-3-3ζ below 56.1°C (Supplemental Table 1). Best hits of ebselen and thimerosal, which show consistent DSF-monitored concentration-dependent effect, are specifically marked (insets). (C) Concentration-dependent DSF for the effect of ebselen (0–5 μM) on the thermal stability of 14-3-3ζ (n = 3; independent DSF measurements). (D) CD spectra of ebselen-treated (blue) and untreated (red) 14-3-3ζ. See *Materials and Methods* for details on data analysis. AU, arbitrary fluorescence unit.

[^{32}P]pSer19TH throughout the experiment and was used as 100%. Except when otherwise indicated, ebselen and ebselen oxide–treated 14-3-3 proteins were prepared by incubating purified 14-3-3 proteins (without any reducing agents) with a 10-fold molar ratio ebselen:14-3-3 subunits on ice for 30 minutes, followed by gel filtration to remove excess of compound. Once modified, the T_m values of the proteins were stable at 4°C for at least 6 hours and after several cycles of freezing and thawing.

Differential Scanning Fluorimetry and Differential Scanning Fluorimetry–Monitored Screening

For differential scanning fluorimetry (DSF)-based screening, the Agilent Bravo Automated Liquid Handling Platform was used for liquid handling. The final screening volume was 10 μl, with 0.1 mg/ml 14-3-3 in 20 mM HEPES and 200 mM NaCl (pH 7.4) and a compound concentration of 400 μM and 4% DMSO in 384-well plates, with 24 DMSO (4%) controls in each plate. SYPRO Orange 5× (Sigma) was used to monitor protein unfolding in Roche LightCycler 480. Unfolding curves were recorded with 0.2°C intervals with a scan rate of 2°C/min from 20 to 95°C, with four acquisitions per degree including a 10-second hold at 20°C before and after the experiment, and were monitored at $\lambda_{excitation}$ = 465 nm and $\lambda_{emission}$ = 610 nm. The experimental unfolding curves were normalized to fraction of unfolded protein and analyzed to extract the T_m values for the protein without (DMSO controls) and with compounds (Urbaneja et al., 2017). T_m values (average ± S.D.) were calculated for 24 DMSO controls. ΔT_m values were calculated as the T_m for the protein with compound minus the T_m value for DMSO control. Any compounds above or below the ±10 × S.D. (for DMSO control) cutoff value were selected as hits for further validations.

The first validation of the initial hits was performed by concentration-dependent DSF by measuring 20 points between 0–400 μM and 0–16 μM (n = 4). DSF experiments with other 14-3-3 isoforms (γ, η, and ε) and 14-3-3ζ mutants were carried out at the same conditions as above. The effect of ebselen on the time-dependent unfolding of 14-3-3ζ was measured by monitoring the increase in SYPRO Orange fluorescence at 37°C for 17 hours with measurements of 2 minutes and 17 seconds each using the same conditions as for DSF, with 0.1 mg/ml of ebselen-treated and untreated 14-3-3ζ (n = 3). The final 14-3-3 protein concentration in these experiments was 0.1 mg/ml (3.7 μM subunit concentration with 2% DMSO in the controls), and the final ebselen concentration was 200 μM (with 2% DMSO).

Circular Dichroism

Circular dichroism (CD) spectra were acquired with a JASCO J-810 spectropolarimeter. CD buffer conditions were 10 mM K_2HPO_4 and 150 mM KF, pH 7.4, at 0.2 mg/ml of ebselen-treated (see above) and untreated 14-3-3ζ. Quartz cuvettes with 0.1-cm path length were used. The samples were measured at 25°C, covering a range of 180–260 nm with a scan rate of 50 nm/min, data pitch of 0.5 nm, response of 0.25 seconds, sensitivity of 100 mdeg, and three accumulations with a bandwidth of 1 nm. The data pitch was 0.2°C and sensitivity was 100 mdeg, with a response of 1 second with a bandwidth of 1 nm. The mean residual ellipticity was determined using the formula $[\theta]mrw = \theta/(n \cdot c \cdot l)$, where θ is the ellipticity (mdeg), c is the protein concentration (M), n is the number of amino acids, and l is the path length of the cuvette (centimeters). Three parallels were averaged after subtraction of baseline spectra and calculation of mean residual ellipticity. Circular dichroism by neural networks (Böhm et al., 1992) was used to estimate secondary structure content.

Surface Plasmon Resonance

Unless otherwise stated, the method below is the same for all surface plasmon resonance (SPR) experiments. The Biacore T200 instrument (GE Healthcare Life Sciences) was used. Immobilization of full-length 14-3-3ζ (1 mg/ml) was carried out in 10 mM sodium acetate, pH 5.1, onto the CM5 sensor chip (GE Healthcare Life Sciences) using standard amine coupling procedure by using PBS as running buffer. The immobilization protocol was 480 seconds with a flow rate of 7 μl/min followed by 2 hours of baseline equilibration. The observed immobilization was about 15,000 response units. The hit compounds were then tested at eight different concentrations between 0 and 200 μM in running buffer containing 5% DMSO at 25°C, 30 μl/min flow rate, contact time of 60 seconds, and dissociation time of 200 seconds, with a final wash after injection with a 50% DMSO solution. The results were analyzed with the Biacore T200 Evaluation software. The binding of pSer19TH to 14-3-3ζ was measured at 25, 50, and 100 nM of the enzyme. The running buffer was PBS with dissociation time of 2000 seconds and without a final wash step with 50% DMSO solution. The experiments with pSer19TH with ebselen-treated 14-3-3ζ were performed with a running buffer of PBS with 5% DMSO, with dissociation time of 2000 seconds and a final wash step with 50% DMSO solution and solvent correction.

Liquid chromatography with tandem mass spectrometry analysis

Protein pellet (20 μg) from ebselen-treated (see above) and untreated 14-3-3ζ was solubilized and trypsinized at 37°C overnight. Tryptic peptides were desalted and purified using a reverse-phase Oasis HLB μElution Plate (30 μm; 2-mg HLB sorbent; Waters, Milford, MA). After purification of tryptic peptides on Oasis c18 columns, the samples were applied on an liquid chromatography column coupled to an Orbitrap Elite in the collision-induced dissociation (CID) and higher-energy collisional dissociation modes or on an liquid chromatography column coupled to an Orbitrap QExactive. The raw files were analyzed by either Proteome Discoverer software version 2.1.0.81 or Peptide Shaker version 1.16.27 (Vaudel et al., 2015). Three search engines were used—MS-Amanda, Sequest, and XTandem—with a fragment ion mass tolerance of 0.02 Da in higher-energy collisional dissociation mode and 0.6 Da in CID mode and a parent ion tolerance of 10 ppm. Oxidation of methionine and modification of cysteine by ebselen were specified as variable modifications, and a human database was used. Scaffold (version Scaffold_4.8.7; Proteome Software Inc., Portland, OR) was used to validate MS/MS-based peptide and protein identifications.

MALDI-MS

The protein samples were incubated with porcine trypsin (Promega) for 2 hours at 40°C in 50 mM ammonium bicarbonate. MALDI-TOF mass spectra were obtained using an ultrafleXtreme instrument (Bruker Daltonics, Bremen, Germany) operated in linear and reflectron positive ion detection modes for analysis of intact mass of the protein and after proteolysis by trypsin, respectively. The identity of the tryptic peptides was verified by means of MALDI-MS/MS.

Cell Culture

SHSY5Y cells [CRL-2266 (SH-SY5Y); RRID: CVCL0019; American Type Culture Collection] from LGC Standards GmbH, Germany, authenticated August 2019 by short-tandem repeat DNA profiling and used at a maximum of 16 passages, were grown in Dulbecco's modified Eagle's medium with 10% fetal bovine serum and 2 mM glutamine. In total, 1.2 × 10^6 SHSY5Y cells per p60 plate were seeded, and 5 hours later, cells were treated with 2–20 μM ebselen or ebselen oxide and DMSO (0.05%) as a control (without ebselen/ebselen oxide). Cells were collected 18 hours post-treatment.

Immunofluorescence on SHSY5Y Cells

In total, 20,000 SHSY5Y cells per well were seeded on coverslips in four-well plates and, 5 hours later, were treated with 5 μM ebselen and DMSO (0.05%). Cells were then incubated for 18 hours before subjecting to immunofluorescence investigation. Cells were fixed with 4% paraformaldehyde for 30 minutes at room temperature and

then permeabilized with PBS 0.2% Triton and blocked with 5% FBS in PBS. Primary antibody rabbit anti–pan-14-3-3 (1:100; Santa Cruz) and mouse anti–β-actin (1:100; Sigma) and secondary antibody anti-rabbit Alexa Fluor 488 (A-11008, RRID: AB_143165; 1:200; Molecular Probes) and anti-mouse Alexa Fluor 555 (A-21422, RRID: AB_141822; 1:200; Molecular Probes) were used. DAPI (Molecular probes) was used as a nuclear stain. Images were obtained by using Leica microscope TCS SP5 (Leica Microsystem GmbH).

Lysate Preparation

Lysates from SHSY5Y cells and zebrafish brain tissues (see below) were prepared in lysis buffer (20 mM HEPES, pH 7.0, 10 mM KCl, 1% NP40) containing protease and phosphatase inhibitor. Triton X-100 (1%) was applied to the brain lysates prior to 30 minutes of incubation at 4°C. Lysates were centrifuged at 10,000 rpm for 10 minutes at 4°C, supernatant was collected, and protein concentration was measured by using direct detect spectrometer (Merck).

Western Blotting

Lysates of SHSY5Y cells or zebrafish brain tissue (5 μg protein) were separated in 10% TGX gels (Bio-Rad) and transferred onto PVDF membrane (Bio-Rad) using the Transblot system (Bio-Rad). Western blotting membranes were incubated with rabbit anti–pan-14-3-3 (sc-629, RRID: AB_2273154; 1:1000; Santa Cruz Biotechnology) as primary antibody. Mouse anti–β-actin (A1978, RRID: AB_476692; 1:1000; Sigma-Aldrich) or rabbit anti-GAPDH (ab9485, RRID: AB_307275;1:1000; Abcam) was used as loading control, and goat anti-rabbit (170-6515, RRID: AB_11125142; 1:1000; Bio-Rad) and goat anti-mouse (170-6516, RRID: AB_11125547; 1:1000; Bio-Rad) were used as secondary antibodies. Ebselen-treated samples were referenced to untreated, which were given the arbitrary value of 1.

For experiments on 14-3-3 degradation in cells, 500,000 SH-SY5Y cells per well were seeded in six-well plates; 5 hours postseeding, cells were treated with 5–10 μM ebselen or ebselen oxide and 50 μM Z-VAD-FMK (caspase inhibitor; Adooq Biosciences) and DMSO (0.05%) as a control (without ebselen and caspase inhibitor). Cells were incubated for 16 hours before treating with 500 nM bortezomib (proteasome inhibitor; Fisher Scientific) for 2 hours before collecting for Western blot analysis. Densitometric analysis was performed using Image Laboratory Software 6.0.1 (Bio-Rad).

Zebrafish Strains, Care, and Maintenance

AB wild-type adult zebrafish (originally from the Zebrafish International Resource Centre; RRID: ZIRC_ZL1) were maintained at the University of Leicester using standard protocols for keeping zebrafish and in accordance with institutional guidelines for animal welfare. They were fed twice per day with ZEBRAFEED 400–600 dry food (Sparos). Zebrafish used for behavioral analysis were randomly netted from a large home tank containing approximately 40 fish, including a mixture of 3-month-old male and female AB wild types. All zebrafish experiments have been approved by the local Animal Welfare and Ethical Review Board and are covered by a UK project license to Dr. Norton (PPL P56FB749).

For experiments with zebrafish brain tissue, ebselen was diluted in system water and applied to AB wild-type zebrafish by immersion for 30 minutes before behavioral testing and for 18 hours before dissection for Western blot analysis. Treatment duration and concentrations were chosen according to pilot experiments in our laboratory. In initial screening experiments, we tested ebselen concentrations between 1 and 5 μM to make conditions comparable with cell culture experiments. At 5 μM ebselen, we observed approximately 50% lethality of the zebrafish, whereas at 1 and 1.5 μM, all fish survived during the observation period, without obvious symptoms of distress. In accordance with animal welfare regulations, we decided to limit the subsequent experiments to a fixed concentration of 1 μM and group sizes of three individuals. At this concentration, we observed consistent behavioral effects without any lethality. Three adult zebrafish were used for Western blotting. They were anesthetized with MS222 and sacrificed by decapitation. The brains were quickly dissected in PBS and frozen in liquid nitrogen.

Behavior Experiments

All behavioral experiments were carried out between 11:00 and 17:00. Experiments were performed in a dedicated room with light and temperature kept constant. These behavioral experiments are classified as mild on our project license. We minimized any potential suffering by maintaining zebrafish in oxygenated water at the correct temperature of 28°C during the experimental period. The graphical timeline of the study was as follows:

No animals were excluded or died during the behavior experiments

Visually Mediated Social Preference for Novelty. The social preference for novelty experiment was performed in a transparent rectangular tank composed of five chambers. One central chamber (19 × 13 cm) was surrounded by four identical chambers (9.5 × 6.5 cm). The transparent walls dividing the chambers contained perforated holes to permit water to move between compartments. For the social preference test, three female adult zebrafish were used as a social stimulus. Their behavior was not included in the data presented here. They were placed in the top-left chamber and left to habituate to the novel setting for 5 minutes. A mixture of 10 male and female adult zebrafish were recorded as focal animals. These test fish were placed individually in the central chamber, and their behavior was recorded for 5 minutes from above. The videos were then analyzed to measure time spent swimming and freezing, which were the primary and secondary endpoints of this study. The zebrafish treated with ebselen were exposed to 1 μM for 30 minutes. Control zebrafish were immersed in 0.01% DMSO. No exclusion criteria were used in this test, meaning that all animals tested were included in the statistical analysis.

Novel Tank Test and Open Feld Test. Tests were performed in a standard 1.5-L trapezoid tank (Egan et al., 2009) (novel tank test) or a large rectangular arena (43 × 22 × 8 cm). A mixture of 10 male and female adult zebrafish were placed individually into the tank and recorded for 5 minutes. EthoVision software (EthoVision XT, RRID: SCR_000441; Noldus) was used to measure locomotion and the amount of time spent freezing. No exclusion criteria were used in this test, meaning that all animals tested were included in the statistical analysis.

Statistical Analysis and Study Design

Triplicate measurements with different sample preparations were performed, and either representative spectra or resulting values as means ± S.D. are provided in the text or in the figure legends. The two-tailed Student's t test and Welch's two-tailed t test were used to evaluate significant differences between the samples. For Western blot–based analyses with lysates from neuroblastoma cells and zebrafish, treated samples were referenced to untreated samples, which were given the arbitrary value of 1. All data are presented as means ± S.D. of measurements with at least three independent cell culture preparations. Assessments of normality of the data were done using the Shapiro-Wilk test. Statistical signification was analyzed by Student's t test (two-tailed) or one-way ANOVA with the Holm-Sidak method. For the behavioral studies with zebrafish, we used 10–12 zebrafish, as indicated, for both the social preference for novelty and novel tank diving assay. This sample size was selected based upon a power analysis using recently reported data (Dalla Vecchia et al., 2019). No blinding was performed. After recording, behavior was analyzed using EthoVision XT tracking software, permitting unbiased comparison of results between treatment groups. All animals were included in the analysis. Zebrafish were then killed using a schedule 1 procedure: overdose of MS222 followed by decapitation as specified by the Animals (Scientific Procedures) Act 1986. Data

were first assessed for normality using the Shapiro-Wilk normality test. We did not test for or remove outliers. Statistical analyses were performed using a Mann-Whitney U test or an unpaired Student's t test with Welch's correction. Statistical analyses were performed using the software GraphPad Prism 8.1.1 (RRID: SCR_002798; GraphPad Prism) and SigmaPlot 13.1 (RRID: SCR_003210; SigmaPlot), and statistical significance was set at $P < 0.05$ for all experiments.

Results

DSF-Based Screening for Drugs Targeting 14-3-3ζ. Identification of Ebselen as a Destabilizer that Covalently Bonds to 14-3-3ζ. To identify compounds capable of binding to 14-3-3ζ, a DSF-based high-throughput screen was carried out using an established protocol for identification of binders to protein targets (Niesen et al., 2007; Aubi et al., 2015; Urbaneja et al., 2017). A similar technique has previously been used to identify peptide stabilizers of 14-3-3 proteins (Valenti et al., 2019). The Prestwick Chemical Library, containing 1280 compounds, 95% of which are approved drugs, was screened. The midpoint melting temperature (T_m) of control samples of 14-3-3ζ with 4% DMSO was 61.1 ± 0.5°C, in agreement with T_m values previously measured for this protein by thermal-dependent CD (Ghosh et al., 2015). Hits were identified based on the change in T_m for the protein (ΔT_m). An absolute value for the change in Tm ($I\Delta T_mI$) ≤ [10 × S.D. (for the DMSO controls)] was selected as the cutoff value for hit identification. Only destabilizing drugs were identified for 14-3-3ζ, and 15 drugs that decreased the T_m of 14-3-3ζ below 56.01 ± 0.5°C ($I\Delta T_mI \geq 5.1 \pm 0.5$°C) were selected as primary hits (Fig. 1B; Supplemental Table 1). These 15 hits were subjected to detailed concentration-dependent DSF analyses at concentrations up to 125 μM. Thimerosal and ebselen showed the most consistent concentration-dependent binding curves at these conditions, with large maximal ΔT_m values (−11.6 ± 0.2°C and −8.1 ± 0.2°C, respectively; Fig. 1B), without inducing 14-3-3ζ denaturation. The organomercury antiseptic compound thimerosal was, however, excluded from further studies on effects on 14-3-3 proteins because of its associated cytotoxicity (James et al., 2005; Parran et al., 2005), and ebselen was pursued as the primary hit compound to understand its destabilizing effect and possible interference on partner binding to 14-3-3ζ. The concentration of ebselen that provided a half-maximal decrease in ΔT_m was defined as the EC_{50}, estimated to be 1.50 ± 0.30 (S.D.) μM for the interaction of ebselen with 14-3-3ζ (Fig. 1C). The effects of ebselen on 14-3-3ζ conformation were studied by CD spectroscopy. The CD signal was slightly lower after ebselen treatment (Fig. 1D). 14-3-3ζ is a largely α-helical protein (Fig. 1A), and accordingly, the percentage of α-helix calculated using circular dichroism by neural networks (Böhm et al., 1992) for untreated and ebselen-treated 14-3-3ζ was approximately 86.4% ± 0.8% and 78.6% ± 1.2%, respectively. These results indicate that the destabilization of the protein caused by ebselen triggers a discrete conformational change of 14-3-3ζ and is not associated with a large denaturation.

Ebselen Covalently Attaches to All Cysteine Residues in 14-3-3ζ, and Modification of C94 Induces Protein Destabilization. The interaction between 14-3-3ζ and ebselen was further validated by SPR. The sensorgram shows that ebselen covalently attaches to the protein and does not dissociate at concentrations up to 25 μM, when a plateau is reached for the response signal quantified in resonance units, suggesting covalent bonding (Fig. 2A). Ebselen has previously been shown to modify protein targets mainly through covalent interaction with cysteine residues (Favrot et al., 2013; Joice et al., 2013; Lieberman et al., 2014; Mukherjee et al., 2014). To investigate the possible involvement of cysteines in ebselen-induced destabilization of 14-3-3ζ, we prepared Cys mutants that were analyzed by mass spectroscopy (MS) to identify cysteine residues modified by ebselen treatment of 14-3-3ζ. Using MS/MS with CID detection, we detected ebselen derivatized by selenylsulfide bonds to tryptic peptides containing either C25, C94, or C189. The identification of a peptide with C94 is illustrated in Fig. 2B. Detailed liquid chromatography-tandem MS and MALDI-TOF MS experiments using the mutants C25A-C189A-14-3-3ζ (Fig. 2C; Supplemental Fig. 2A) and C94A-14-3-3ζ (Fig. 2D; Supplemental Fig. 2B) contributed to identify C25 as the preferential site of ebselen conjugation with high confidence, followed by C94 and C189. A preferential *S*-glutathionylation (Kim et al., 2014) and *S*-nitrosylation (Greco et al., 2006) labeling of C25 in 14-3-3ζ has also been previously reported.

We also investigated the thermal stability of the Cys mutants by DSF (Table 1). It has been shown that the buried C94 is a determinant for the stability of 14-3-3ζ (Jandova et al., 2018). Accordingly, we noted a protein destabilization caused by mutation of C94, observed in the single mutant C94A and in the double (C25A-C94A and C94A-C189A) and triple mutants, which presented a decrease in T_m of 3.2–5.9°C compared with wild-type (WT)-14-3-3ζ (Table 1). On the other hand, mutations at C25 and C189 did not affect the protein stability, as seen with the C25A and C25A-C189A mutants (Table 1). With respect to the ebselen effect, both triple mutants (C25A-C94I-C189A and C25A-C94V-C189A) were unaffected by ebselen treatment, which excluded the possibility that the destabilization originated from modification of 14-3-3ζ at other residues than cysteine. The results also indicate that ebselen induced only minor changes in T_m in C94-mutants, whereas the two mutants at other residues, but with C94 intact (C25A and C25A-C189A), showed a similar destabilization (8.6–9.0°C decrease in T_m) as WT-14-3-3ζ (Table 1), pointing to C94 as the site for ebselenation-mediated destabilization.

Altogether, the MS analyses of 14-3-3ζ and Cys mutants revealed a complex pattern of Cys modification by ebselen, which appeared to occur at all Cys residues, but to a larger degree for C25 and a lesser extent for C94 and C189, whereas the DSF assays of mutated proteins (Table 1) indicate that the destabilization is dependent on the ebselen modification of C94.

Ebselen Modification of 14-3-3ζ Affects Its Kinetic Stability and Its Interaction with pSer19TH. Based on the discrete destabilization of 14-3-3ζ observed by ebselen treatment, leading to an approx. 7°C reduction in T_m (see above and Table 1), it is not straightforward to predict subsequent physiologic consequences of ebselen modification. By measuring the fluorescence-monitored isothermal loss of conformational stability of the protein at 37°C, we observed a severalfold increased rate of unfolding for the ebselen-treated 14-3-3ζ compared with the untreated control (Fig. 3A). This indicates that the protein may show altered stability also at physiologic conditions. The functional consequences of the

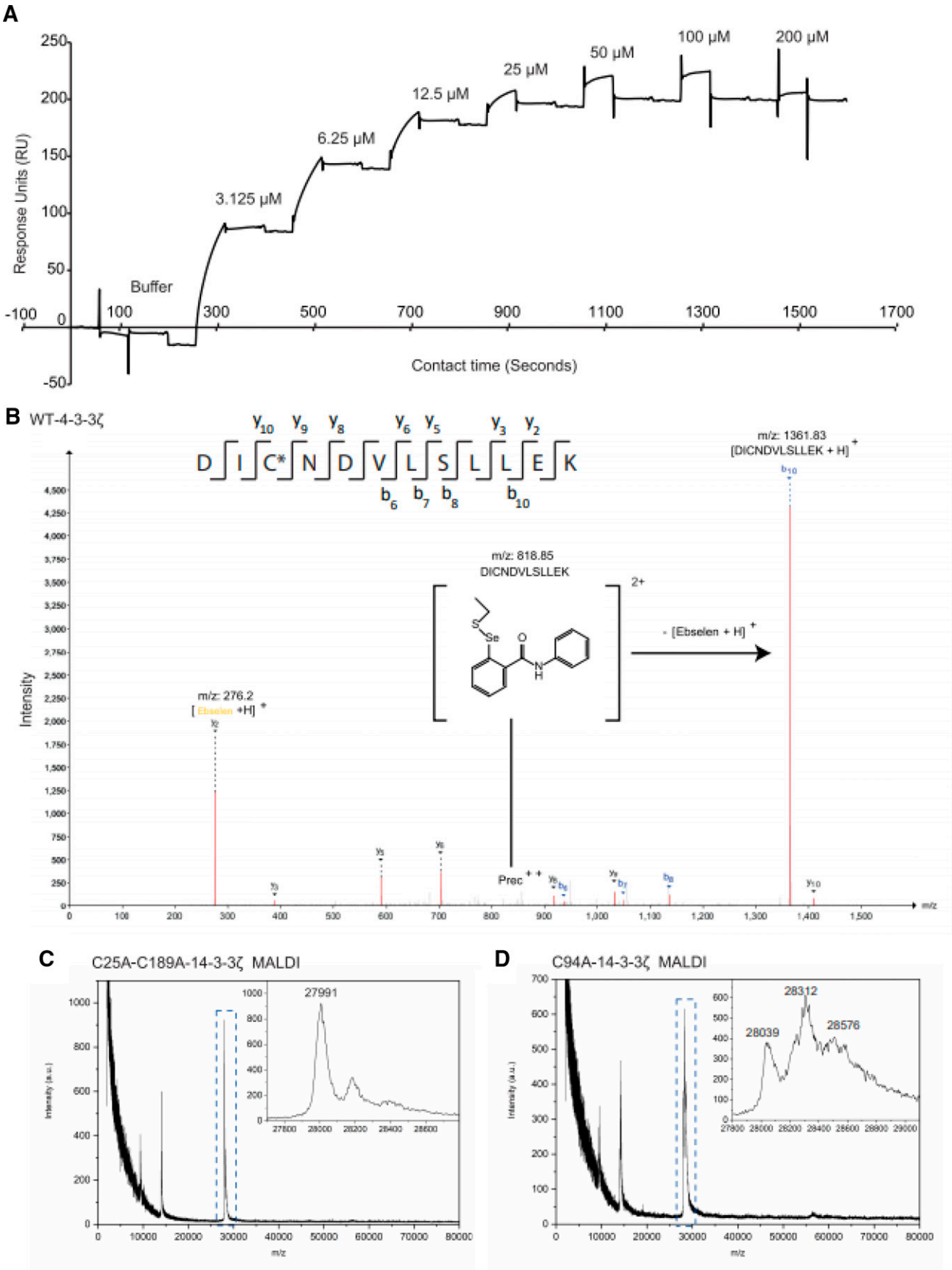

Fig. 2. Covalent bonding of ebselen to 14-3-3ζ and identification of interacting cysteine residues. (A) SPR sensorgram is presented for the interaction of ebselen with immobilized 14-3-3. The concentrations of ebselen added ranged from 0 to 200 µM. (B) Positive ion CID MS/MS mass spectrum of ebselen (m/z = 275 Da) and ebselenated peptide containing C94 [DIC*NDVLSLLEK + 2H]$^{2+}$ (m/z: 818.85). The asterisk denotes

TABLE 1
Effect of ebselen on the midpoint melting temperatures (T_m) of 14-3-3ζ (wild-type and cysteine mutants)

14-3-3ζ-	T_m (−Ebselen)	T_m (+ Ebselen)	ΔT_m (+ Ebselen) − (−Ebselen)
		°C	
Wild-type	60.1 ± 1.3	53.1 ± 1.3	−7.0 ± 1.3
C25A	59.9 ± 0.1 (−0.2 ± 0.6)*	50.9 ± 0.8	−9.0 ± 0.9
C25A-C94A	56.3 ± 0.4 (−4.8 ± 0.5)	53.5 ± 0.8	−2.8 ± 1.2
C25A-C189A	59.2 ± 0.3 (−0.7 ± 0.8)	50.6 ± 0.6	−8.6 ± 0.9
C25A-C94I-C189A	57.9 ± 0.3 (−3.2 ± 0.8)	57.6 ± 0.1	−0.3 ± 0.4
C25A-C94V-C189A	57.3 ± 0.4 (−3.8 ± 0.9)	56.9 ± 0.1	−0.4 ± 0.5
C94A	56.3 ± 0.1 (−4.8 ± 0.6)	55.5 ± 1.1	−0.8 ± 1.2
C94A-C189A	55.2 ± 0.3 (−5.9 ± 0.8)	56.5 ± 1.7	−1.3 ± 2.0

*In parenthesis, the difference between T_m values for nontreated (−Ebselen) mutants of 14-3-3ζ and wild-type 14-3-3ζ.

destabilizing conformational change of 14-3-3ζ was explored by examining its interaction with a physiologically relevant protein partner. To this end, we measured the binding of the archetypical 14-3-3 partner pSer19TH to ebselen-treated and untreated 14-3-3ζ by SPR. Complex formation of pSer19TH with 14-3-3 proteins is of high affinity and activates and stabilizes TH (Ghorbani et al., 2016). As seen in Fig. 3B, the binding of ebselen-treated 14-3-3ζ to pSer19TH was reduced compared with the untreated protein.

Ebselen Destabilizes Several 14-3-3 Isoforms. We further investigated whether the destabilizing effect of ebselen on 14-3-3ζ could also be observed for other 14-3-3 isoforms. All these proteins have conserved Cys residues at positions equivalent to C94 in the ζ isoform; C189 is conserved in all isoforms except in σ, and C25 is not conserved (Supplemental Fig. 1). 14-3-3η showed the lowest thermal stability (T_m = 47.9 ± 0.2°C), followed by 14-3-3γ (56.9 ± 0.2°C), whereas 14-3-3ε (59.7 ± 0.1°C) and 14-3-3ζ (59.9 ± 0.3°C) had similar T_m values. All tested isoforms were destabilized by ebselen; however, in contrast to 14-3-3ζ, ebselen treatment did not elicit a discrete destabilizing conformational change in these isoforms but, rather, a major destabilization, as observed for the ε and γ isoforms, or denaturation for η (Fig. 3C; Table 1; data not shown). Curiously, a concentration-effect threshold was seen at low concentrations of ebselen in the concentration-dependent destabilization (ΔT_m values) for 14-3-3 ζ (Fig. 3C), which was not observed in the other tested isoforms, and 14-3-3ζ was also the most resilient isoform against the destabilizing effects of ebselen. The apparent concentration threshold of 14-3-3ζ modification may indicate that an intact C25 exerts a stabilizing effect on this protein. Only when C25 has been modified would the consecutive bonding of ebselen to C94 lead to destabilization of the ζ isoform.

We have reported that the interaction between pSer19TH and 14-3-3 is conserved between different isoforms, but that 14-3-3γ had the strongest effect on activation and inhibition of pSer19TH dephosphorylation (Ghorbani et al., 2016). 14-3-3 proteins also modulated access to other regulatory sites for multisite phosphorylation of TH (Ghorbani et al., 2020). As inhibition of TH dephosphorylation is a sensitive functional readout of 14-3-3, we conducted dephosphorylation experiments with ^{32}P-labeled pSer19TH in the presence or absence of 14-3-3γ, or 14-3-3γ pretreated with ebselen or ebselen oxide (Fig. 3D). PRAK phosphorylated TH (pSer19TH) was stably labeled throughout the dephosphorylation experiment, as shown in the absence of added phosphatase (Fig. 3D), and was rapidly dephosphorylated in the absence of unmodified 14-3-3γ, which inhibited dephosphorylation substantially. This was however not the case for ebselen-treated 14-3-3, which showed no significant inhibition compared with no 14-3-3, whereas ebselen oxide–treated 14-3-3 showed some residual inhibition (Fig. 3D).

In conclusion, it appears that 14-3-3 isoforms behave differently in the presence of ebselen, and these differences can be hypothesized to be due to differences in cysteine residues within the protein.

Ebselen Treatment of SHSY5Y Cells Triggers Proteasomal Degradation of 14-3-3. To test the effects of ebselen on 14-3-3 protein stability and turnover in intact cells, we performed immunofluorescence imaging of SH-SY5Y cells treated with ebselen. After evaluating the viability of the cells at different ebselen and DMSO concentrations, 5 μM ebselen with 0.05% DMSO was selected, using untreated as well as a DMSO control (0.05%) cells for comparison (Fig. 4A). The levels of DAPI, 14-3-3, and β-actin were virtually unchanged for the untreated and DMSO control cells. However, the 14-3-3 signal was significantly reduced in cells treated with ebselen. This was confirmed by Western blotting experiments and densitometric analysis, showing that ebselen-treated cells had 28% ± 13% decreased 14-3-3 levels compared with untreated cells (Fig. 4B). To investigate the mechanism for 14-3-3 depletion, cells were

one ebselen tag on the peptide cysteine group. (C) MALDI-TOF mass spectrometry of C25A-C189A-14-3-3ζ mutant after ebselen treatment. Inset: the major peak corresponds to unlabeled mutant (theoretical m/z = 28005 Da); the following peak most probably represents an adduct with the MALDI matrix (ferulic acid, m/z = 180 Da) and ebselen-tagged protein (m/z≈ 28270), which presented low intensity. (D) MALDI-TOF mass spectrometry of C94A-14-3-3ζ mutant tagged with ebselen (see also Supplemental Fig. 2A). Inset: the first peak corresponds to unlabeled mutant (theoretical m/z = 28038 Da), and the following peaks correspond to single- and double-tagged proteins (see also Supplemental Fig. 2B). m/z, ratio of mass/charge. Prec = precursor ion, a.u. = arbitrary units.

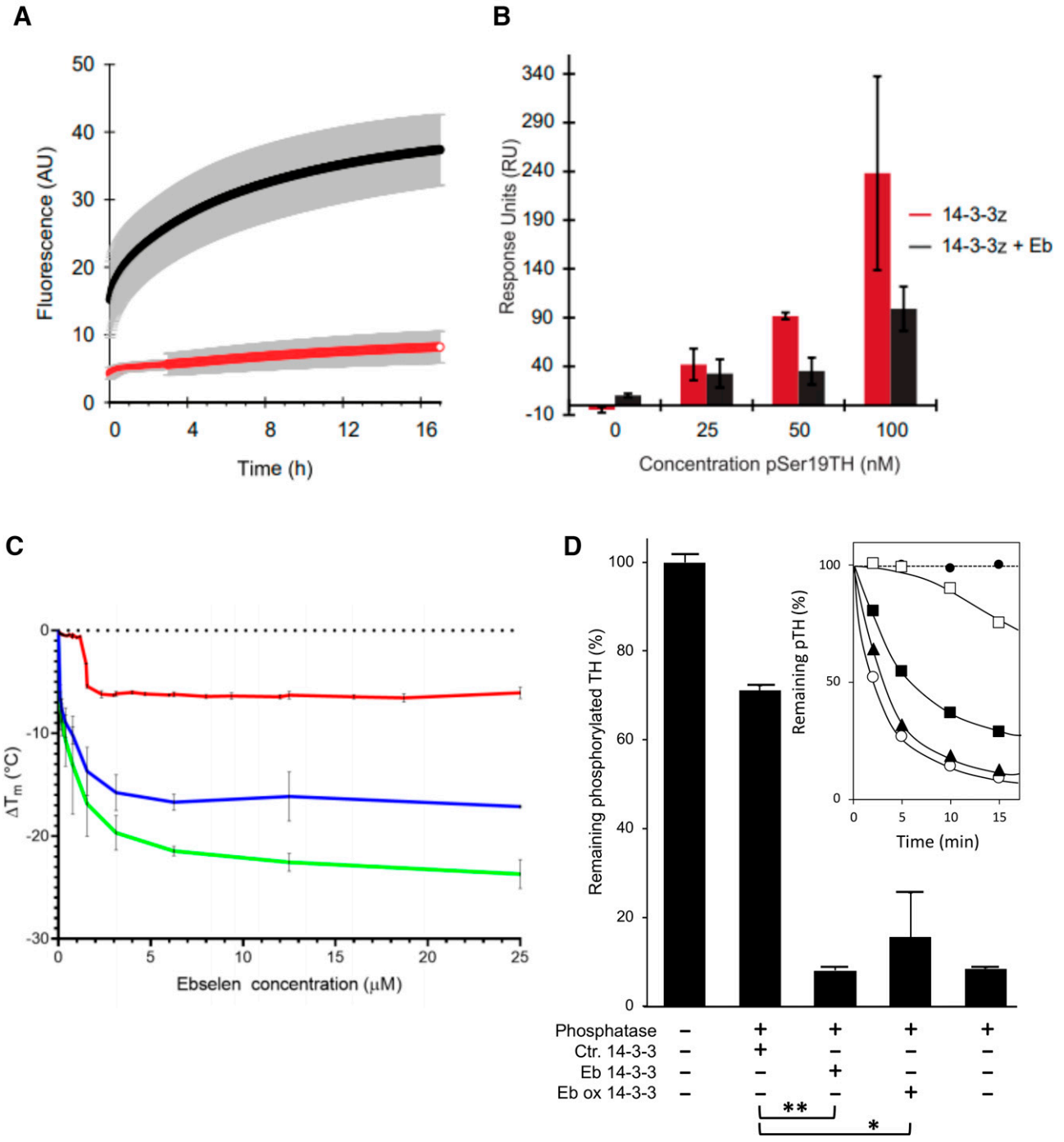

Fig. 3. The effect of ebselen modification on the stability and binding partner interactions of 14-3-3. (A) The kinetic stability of ebselen-treated (black curve) and untreated (red curve) 14-3-3ζ measured by monitoring the time-dependent increase of SYPRO Orange fluorescence (AU, arbitrary fluorescence unit) at 37°C for up to 17 hours, represented as the average of triplicate measurements at each time point, with S.D. in gray. (B) SPR results [recorded response units (RU)] for the binding of pSer19TH to immobilized 14-3-3ζ, either untreated (red bars) or treated (black bars) with ebselen, measured at two concentrations of pSer19TH. Data represent the average (± S.D.) of duplicate measurements with two different preparations of pSer19TH. (C) Concentration-dependent DSF results comparing the melting points of 14-3-3ζ (red), γ (green), and ε (blue) after treatment with ebselen. (D) The effect of 14-3-3γ, ebselen-treated 14-3-3γ (Eb 14-3-3), and ebselen oxide–treated 14-3-3γ (Eb ox 14-3-3) on pSer19TH dephosphorylation. The inset shows the remaining [^{32}P]pSer19 at different time points for samples run in absence of phosphatase (●, dotted line), in the presence of phosphatase, but no 14-3-3 (○), 14-3-3 control (□), ebselen-treated 14-3-3 (△), and ebselen oxide–treated 14-3-3 (□). The bar plot shows the remaining [^{32}P]pSer19 (in %, relative to samples with no phosphatase added) after 10-minute reaction, shown as mean + S.D. (n = 3). P values (t test, two-sided, different variance) of 0.013 (*) and 1.55 10^{-6} (**) were calculated for 14-3-3 control (Ctr. 14-3-3) compared with ebselen- or ebselen oxide–treated 14-3-3, respectively.

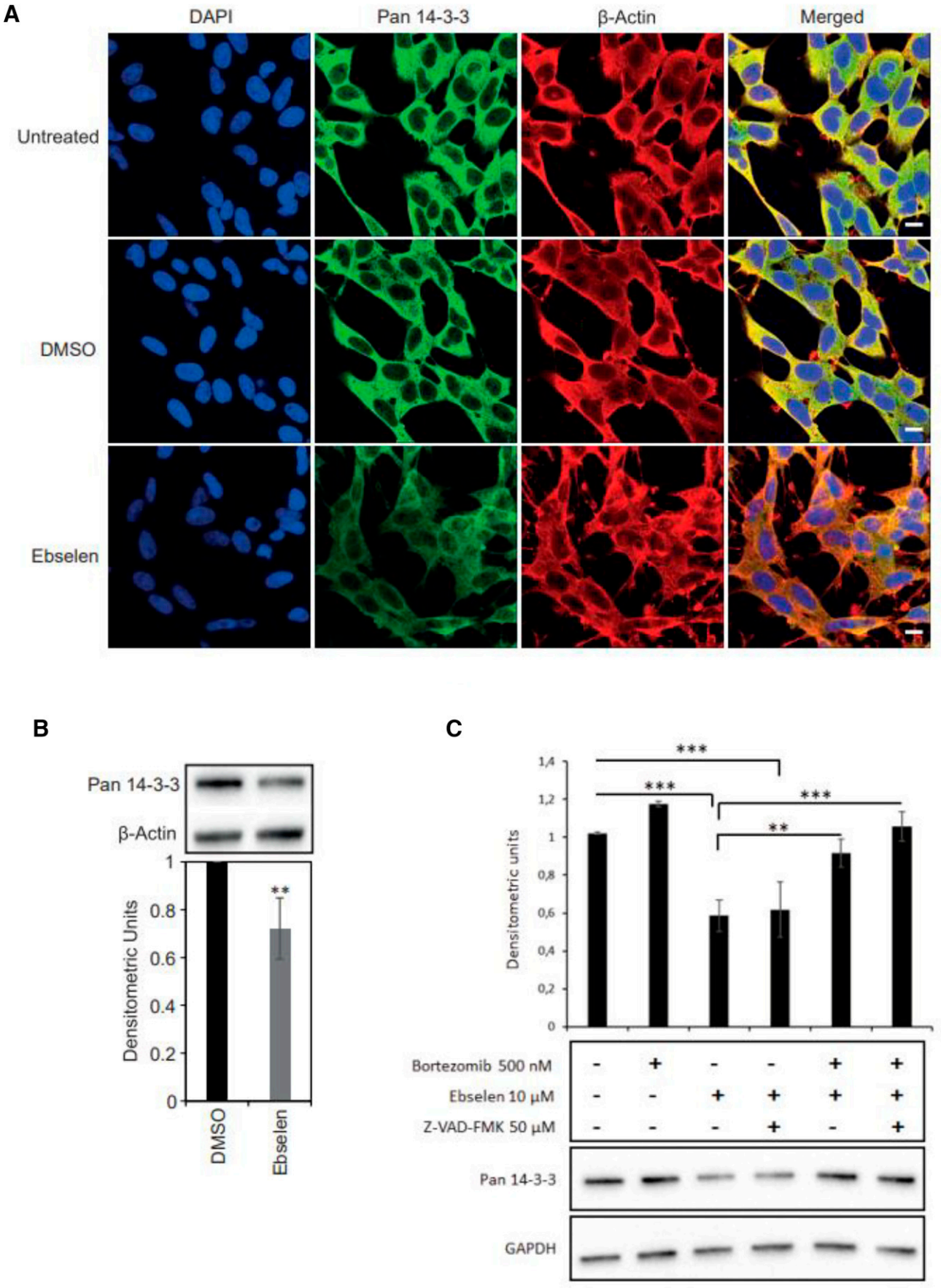

Fig. 4. (A) Immunofluorescence investigation of neuroblastoma cells: untreated and ebselen treated (5 μM in 0.05% DMSO). A DMSO control (0.05%) is also shown. Pan-14-3-3 (green) and β-actin (red) were immunodetected. Nuclei were stained with DAPI. Scale bars, 10 μm. (B) Western blot investigation using SHSY5Y cell samples untreated and treated with ebselen as in (A); 14-3-3 was immunodetected using actin as a

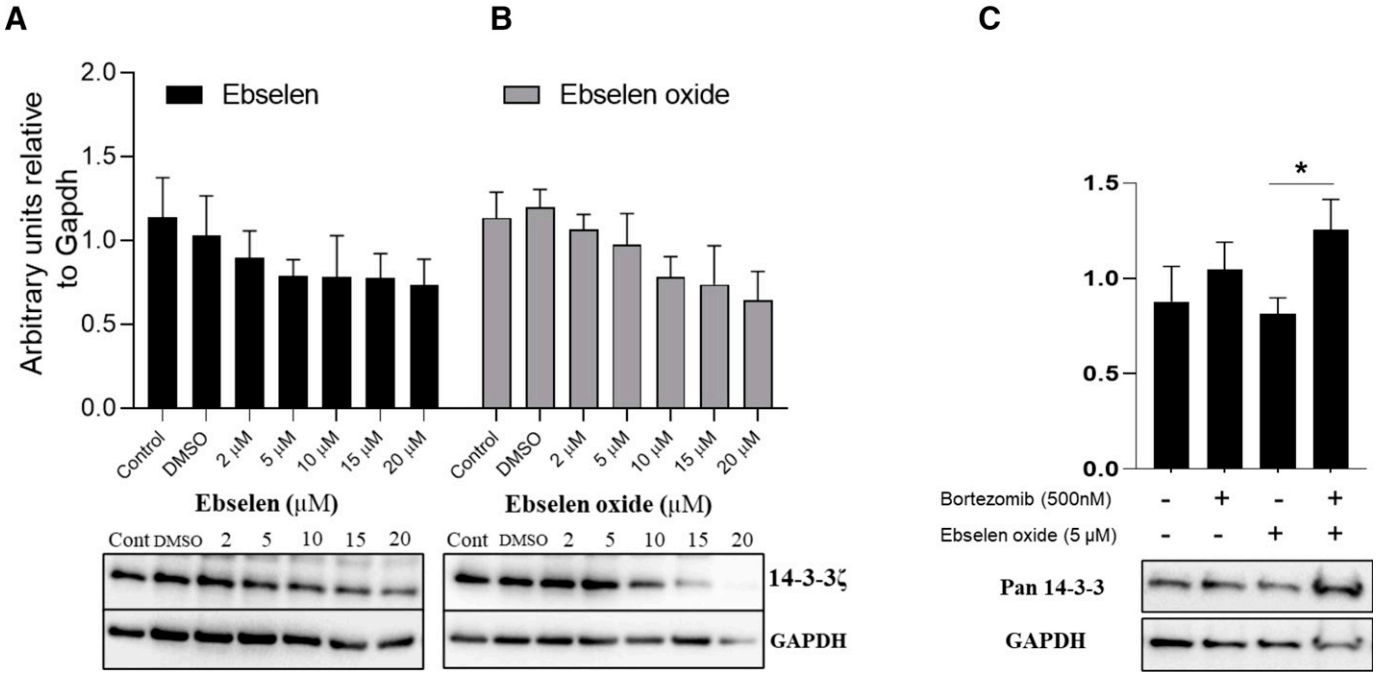

Fig. 5. Effects of ebselen and ebselen oxide on 14-3-3 levels in SHSY5Y cells. Cells were treated with increasing concentrations of ebselen (A) or ebselen oxide (B), showing the reduction of 14-3-3ζ level with increasing concentration of the respective compounds compared with untreated (DMSO control). (C) Western blot of SH-SY5Y cells comparing total 14-3-3 levels upon treatment with 500 nM bortezomib and 5 μM ebselen oxide, showing the reduction of 14-3-3ζ level with ebselen oxide compared with proteasomal inhibitor–treated cells in presence of ebselen oxide. GAPDH was used as a loading reference. Densitometric analysis was used to determine the comparison of the treated samples with the untreated (arbitrarily taken as 1) (n = 5, independent cell culture preparations; $P < 0.05$). Statistical analyses by two-tailed Student's t test. *$P < 0.05$. All data are presented as means ± S.D. Cont = negative control.

treated with ebselen, a proteasome inhibitor (bortezomib), and a caspase inhibitor (Z-VAD-FMK). Cell samples pretreated with ebselen and then treated with either the proteasomal inhibitor or a mixture of proteasomal and caspase inhibitors showed a significant increase in 14-3-3 level compared with cell samples only treated with ebselen. However, samples treated with ebselen and then with the caspase inhibitor showed a similar level of 14-3-3 as the samples treated only with ebselen. These results indicate that ebselen treatment triggers a proteasome-mediated degradation of 14-3-3 in SHSY5Y cells (Fig. 4C).

Comparison of Ebselen and Ebselen Oxide. Previous studies have shown that ebselen can act as an antioxidant and reduce hydroperoxides. During this process, ebselen is converted into the antioxidant inactive derivative ebselen oxide (Lass et al., 1996). To explore whether the cellular effects of ebselen might be mediated by its oxidized derivative, we compared the effects of ebselen and ebselen oxide. As shown in Fig. 5, ebselen and ebselen oxide had slightly different effects on the viability of SHSY5Y cells (Supplemental Fig. 3). At 20 μM ebselen oxide, the cellular viability was reduced by 71%, compared with 41% reduced viability by ebselen at this concentration (P = 0.007, for comparison, t test). However, the effects of ebselen and ebselen oxide on cellular levels of 14-3-3 were rather similar, as reported for other protein targets (Wang et al., 2017). For both compounds, the levels of 14-3-3 proteins gradually decreased at concentrations exceeding 2 μM, and the effects were abolished by treatment with bortezomib. A similar decrease of 14-3-3 levels was observed using either14-3-3ζ-specific antibodies or pan-14-3-3 antibodies, suggesting that the decrease was not limited to one particular isoform. Based on these studies, we conclude that the observed effects of ebselen on intact cells could (partially) be mediated by its oxidized derivative(s).

In Vivo Action of Ebselen in Zebrafish Brain. The effect of ebselen on 14-3-3 proteins was also studied in adult zebrafish. Zebrafish were treated with 1 μM ebselen for 18 hours before the brains were collected. Western blot was performed using the brain lysates of ebselen-treated zebrafish versus untreated (DMSO control). Densitometric analysis showed a significant reduction of 14-3-3 in the brain of zebrafish treated with ebselen compared with untreated control (Fig. 6A). This reduction in 14-3-3 abundance was in accordance with our observation in SHSY5Y cells (Fig. 4).

A visually mediated social preference test was carried out after treatment with 1 μM ebselen for 30 minutes (n = 30) (Fig. 6B) (Carreño Gutiérrez et al., 2019). Zebrafish immersed in 0.01% DMSO control water froze for approximately 25

loading control. Densitometric analysis was carried out to perform the statistical analysis, showing the reduction of 14-3-3 level in ebselen-treated cells compared with untreated (DMSO control arbitrarily taken as 1) (n = 4, independent cell culture preparations, P = 0.004). (C) Western blot of SHSY5Y cells comparing pan-14-3-3 levels upon treatment with 500 nM bortezomib, 10 μM ebselen, and 50 μM Z-VAD-FMK. GAPDH was used as a loading reference. Densitometric analysis was used to determine the comparison of the treated samples with the untreated (arbitrarily taken as 1) (n = 3, independent cell culture preparations; $P < 0.05$). Statistical analyses by two-tailed Student's t test (B) and one-way ANOVA with the Holm-Sidak method (C). *$P < 0.5$, **$P < 0.005$, ***$P < 0.001$. All data are presented as means ± S.D.

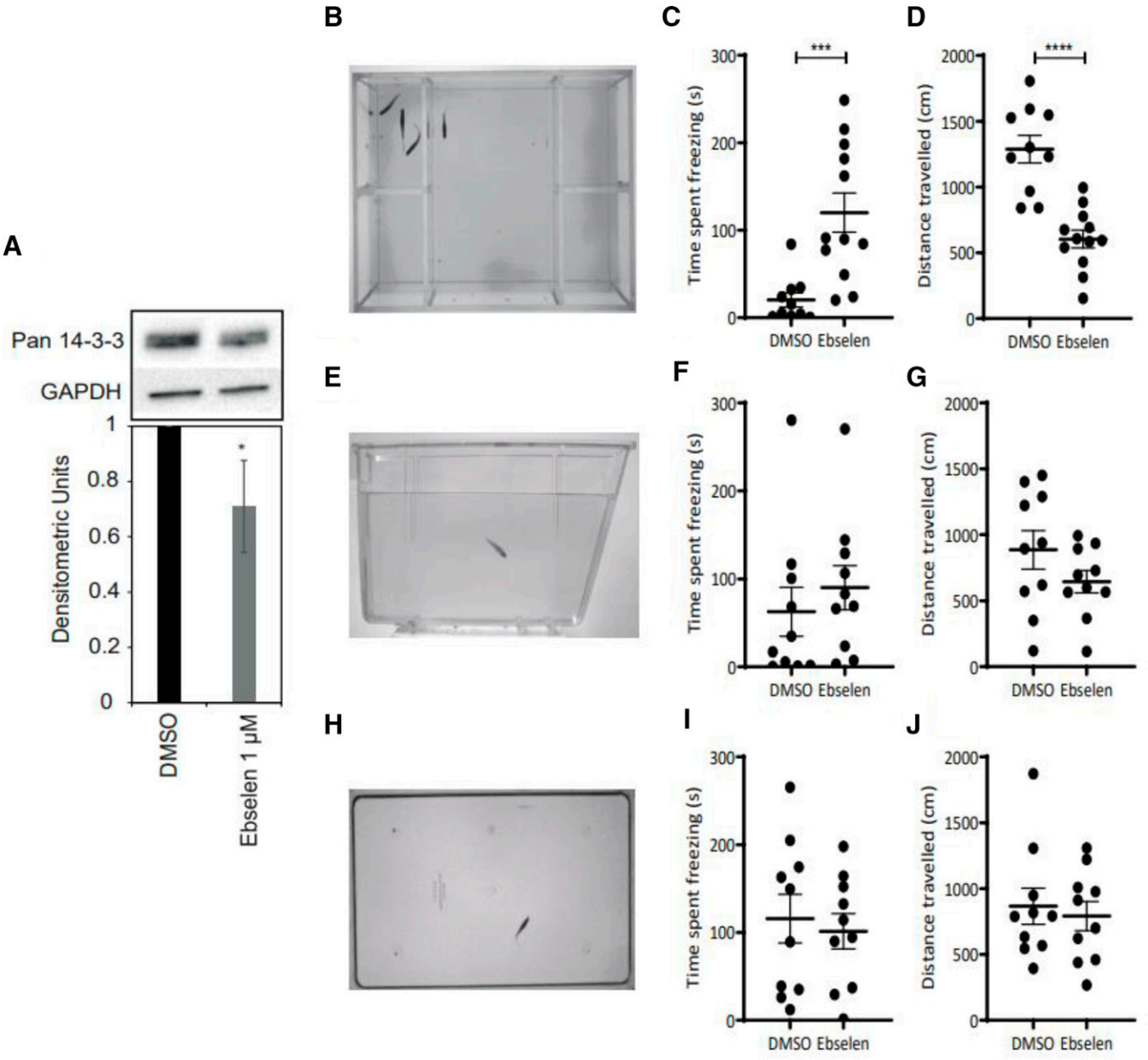

Fig. 6. Effect of ebselen on 14-3-3 abundance in the zebrafish brain and on behavior. (A) Western blot of WT zebrafish brain lysate for DMSO control (0.01%) and ebselen-treated animals (1 μM in 0.01% DMSO). 14-3-3 was immunodetected in the samples with GAPDH as loading control. Densitometric analysis was used to determine the reduction of 14-3-3 abundance in ebselen-treated zebrafish (n = 3, independent lysates of one zebrafish each, $^*P < 0.05$). (B) Tanks used to measure visually mediated social preference. (C) Visually mediated social preference: WT zebrafish spend more time freezing after ebselen treatment compared with DMSO-treated controls (P = 0.0003). (D) Visually mediated social preference: ebselen-treated zebrafish swim significantly less ($P < 0.0001$). Unpaired t test with Welch's correction or Mann-Whitney U test. (E) Tank used in the novel tank test. (F) Freezing behavior is not affected by ebselen treatment in the novel tank test (P = 0.22). (G) Locomotion is not affected by ebselen treatment in the novel tank test (P = 0.18). Unpaired t test with Welch's correction or Mann-Whitney U test. (H) Tank used in the open field test. (I) Freezing behavior is not affected by ebselen treatment in the open field test (P = 0.68). (J) Locomotion is not affected by ebselen treatment in the open field test (P = 0.67). (C and D) n = 10 DMSO controls, and n = 12 for ebselen-treated animals; (F, G, I, and J) unpaired t test with Welch's correction. $^{***}P < 0.001$, $^{****}P < 0.0001$. Means ± S.E.M.

seconds. In comparison, zebrafish treated with 1 μM ebselen froze for more than 100 seconds (Fig. 6C). Moreover, zebrafish treated with DMSO swam for approximately 1250 cm, whereas the ebselen-treated zebrafish only swam about 500 cm (Fig. 6D). The novel tank test (Fig. 6E) and the open field test (Fig. 6H) were also carried out. These tests revealed no significant differences between DMSO and ebselen-treated zebrafish in terms of time spent frozen and distance traveled (Fig. 6, F, G, I, and J). This is similar to previous research reporting that zebrafish treated with lithium display approximately half the mobility of untreated zebrafish (Nery et al., 2014). The lithium effect has been associated to direct binding and inhibition of targets such as glycogen synthase kinase 3β and inositol monophosphatase. Interestingly, inositol monophosphatase is also efficiently inhibited by ebselen (Singh et al., 2013, 2016; Masaki et al., 2016). To

explore this connection, we used a DSF-monitored binding assay to investigate whether lithium would directly bind to 14-3-3ζ. However, no apparent binding was observed when lithium tested in the concentration range of 0.01 μM to 10 mM (data not shown).

Discussion

In this work, we screened a chemical library to find compounds that interact with 14-3-3ζ. This isoform was selected for initial screening because of its high abundance in the central nervous system and strong involvement in human physiologic functions and disorders (Torrico et al., 2020). Strikingly, only destabilizing compounds were found. This is unusual for DSF-based screens, which customarily result in identification of both stabilizing and destabilizing ligands (Niesen et al., 2007; Aubi et al., 2015). The 14-3-3 destabilizing drugs belong to different therapeutic classes, with an over-representation of proton pump inhibitors and calcium channel blockers, several of them including S or Se in their structure (Supplemental Table 1). Ebselen was identified as a destabilizer through covalent bonding to 14-3-3ζ and was similarly shown to modify and destabilize 14-3-3ε, γ, and η, but with markedly large differences between these highly conserved isoforms.

Ebselen is a synthetic seleno-organic compound with several biologic activities including antioxidant, anti-inflammatory, and glutathione peroxidase mimicking activity (Lass et al., 1996; Azad and Tomar 2014). Ebselen has previously been shown to modify protein function through covalent bonding with cysteine residues via its Se atom, forming stable selenenylsulfide (–Se–S–) bonds (Favrot et al., 2013; Mukherjee et al., 2014), as confirmed also here by liquid chromatography-tandem MS for the formation of ebselenated adducts of the modified Cys residues in 14-3-3ζ. Ebselen destabilized 14-3-3ζ, which contains three Cys residues: C25, C94, and C189 (Fig. 1A; Supplemental Fig. 1). We calculated the solvent accessibility of all three Cys residues in 14-3-3ζ using the program Getarea (http://curie.utmb.edu/getarea.html) and all previously published three-dimensional structures of this isoform (PDB: 1QJA, 1QJB, 2C1N, 2O02, 4FJ3, 5D2D, 5EXA, 5NAS, 6F08, and 6FNA, with ligands removed). This analysis showed that C25 and C189 are partially solvent-accessible—2.6%–13.8% (average 7.04%) and 17.6%–30.4% (average 25.17%) in different structures, respectively—whereas C94 was found to be solvent-inaccessible in all structures. Thus, a priori, C25 and C189 would appear to be preferred targets for ebselen modification. However, previous studies have shown that ebselen is also capable of covalently modifying deeply embedded Cys residues (Mukherjee et al., 2014).

A concentration-effect threshold was observed at the lowest concentrations in the concentration-dependent DSF screen of 14-3-3ζ, most probably explained by the stabilizing effect of C25, which is not present in isoforms ε, γ, or η (Supplemental Fig. 1), whereas destabilization appears associated to ebselen modification of C94. Protein destabilization brought about by conformational changes has been previously shown as an effective mechanism of drug action (Ren et al., 2018). In the case of the ebselenated *Mycobacterium tuberculosis* antigen 85 complex, it has been shown that ebselen bonding triggers structural changes accompanied by a decrease in protein thermal stability (Goins et al., 2017). Thus, the CD results support the destabilizing effect of ebselen due to a discrete conformational effect on 14-3-3ζ without denaturing the protein, even after treatment with a high and saturating concentration of ebselen (200 μM).

The functional consequences of the destabilizing conformational change of 14-3-3ζ were demonstrated by showing a decreased interaction with the physiologically relevant protein partner TH. Together with the tryptophan hydroxylases (TPHs) 1 and 2, TH was among the first proteins identified to bind to 14-3-3 proteins (Ichimura et al., 1987). The interaction between 14-3-3 proteins and TH primarily takes place at phosphorylated Ser19 on the N-terminal tail of TH. This phosphorylated amino acid interacts with two conserved Arg residues and one Tyr residue of 14-3-3 within the main binding cleft (PDB: 4J6S) (Skjevik et al., 2014). TH catalyzes the rate-limiting step in the biosynthesis of dopamine. Thus, compounds that modulate the TH-14-3-3 interaction could represent potential therapeutics for disorders related to altered dopamine function, such as attention deficit hyperactive disorder, parkinsonism, and Parkinson disease (Del Campo et al., 2011; Waloen et al., 2017). Similarly, the 14-3-3 regulated enzymes TPH1 and TPH2 catalyze the rate-limiting reaction in the synthesis of serotonin, an important signaling molecule, and these tryptophan hydroxylase-14-3-3 complexes also represent relevant therapeutic targets (Waloen et al., 2017).

We also explored how ebselen treatment influenced 14-3-3 levels in intact cells and tissues. Increased protein instability caused by mutations or chemical modifications usually results in dysfunction and reduction of cellular protein levels due to increased processing of the proteins by quality control systems, notably through the ubiquitin-dependent proteasome system (Vilchez et al., 2014). Caspase-dependent degradation has been reported to be implicated in the reduction of 14-3-3ζ levels after intracellular oxidation (Kim et al., 2014). On the other hand, proteasome-mediated 14-3-3 degradation of the γ isoform has also been reported (Chen et al., 2015).

The function and regulation of 14-3-3 proteins have been studied in several cell types derived from the nervous system, notably the SHSY5Y neuroblastoma cell line. These cells express multiple 14-3-3 isoforms, including 14-3-3ε and ζ, which were of particular interest in our study. It was recently shown that these 14-3-3 isoforms are subject to ubiquitin-regulated proteasomal degradation in SHSY5Y cells (Jiang et al., 2019). Our observation that ebselen treatment triggered ubiquitin-mediated proteasomal degradation of 14-3-3 proteins in SHSY5Y cells (Fig. 4C) is consistent with these findings.

Proteasome-mediated degradation of ebselen and ebselen oxide–modified proteins has previously been reported (Li et al., 2014). It nevertheless is possible that the effect of ebselen on 14-3-3 levels may be indirect, by, e.g., increasing the phosphorylation, ubiquitination, or other covalent modification of 14-3-3 proteins, as such modifications are reported to trigger 14-3-3 degradation (Chen et al., 2015; Jiang et al., 2019).

The 14-3-3 proteins constitute about 1% of total soluble brain proteins (Aitken 2006). They are involved in multiple functions, including metabolic regulation and cortical development (Cornell and Toyo-Oka, 2017). Common and rare genetic variants in 14-3-3 proteins are implicated in multiple

neuropsychiatric disorders, making the 14-3-3 proteins and their protein-partner networks attractive as therapeutic targets in neuropsychiatry (Jacobsen et al., 2015; Pagan et al., 2017; Torrico et al., 2020). The in vivo experiments showed that zebrafish treated with ebselen exhibited a freezing behavior and reduced locomotion (Fig. 6). Similarly, ebselen reduces impulsivity in rodent models and has been suggested as an alternative to lithium in the treatment of bipolar disorder and other mood disorders (Singh et al., 2013, 2016). Lithium has severe side effects, whereas ebselen has limited toxicity at brain-active therapeutic concentrations, which makes ebselen a potentially safer treatment alternative (Singh et al., 2013, 2016). The 14-3-3 proteins regulate the established lithium target glycogen synthase kinase 3β (Liao et al., 2005; Sugden et al., 2008), pointing to crosstalk of protein networks targeted by lithium and by alteration of 14-3-3 functionality. This indicates that alteration of protein interaction networks involving 14-3-3 proteins may contribute to the lithium-mimicking effect of ebselen. Nevertheless, elucidation of the molecular basis for the phenotype caused by ebselen treatment requires further investigation. Moreover, because of the broad and rather nonspecific effects of ebselen, it is very probable that other molecular targets are also involved in its lithium-mimicking activity. Interestingly, we did not observe any direct binding of lithium to 14-3-3ζ at therapeutically relevant concentrations.

Overexpression of 14-3-3 has been found in several cancer forms and is associated with poor prognosis and aggressive tumor growth (Liu et al., 2014; Xiao et al., 2014). Reduction of 14-3-3 abundance makes cancer cells more susceptible to chemotherapy treatment, and 14-3-3 proteins are considered attractive targets for cancer therapy (Cao et al., 2015; Woodcock et al., 2015). Thus, the ebselen effect on 14-3-3 turnover and consequent alteration of the PPI network is also expected to be relevant for cancer treatment. Actually, cysteine residues in 14-3-3 are targets of photodynamic light cancer therapy mediated by reactive oxygen species, and oxidization of these residues is expected to mediate the apoptosis triggered by such treatment (Helander et al., 2016). Our work, showing the ability of ebselen to reduce the abundance and function of 14-3-3 in vivo through cysteine modification, also reinforces the promise of ebselen as an exciting candidate to use in cancer treatment in addition to mood disorders. Furthermore, this study also identified 15 other small-molecule drugs with destabilizing effects on 14-3-3ζ (Supplemental Table 1). These compounds share redox activity properties with ebselen and most include S atoms, indicating that their destabilizing effects on 14-3-3 proteins may also be mediated by interaction with cysteine residues. As ebselen is a redox active compound, its effects may be modified in cells and in vivo by glutathione, free cysteine, or other cellular sulfhydryl compounds by reducing the selenylsulfide bonds.

In summary, the destabilizing effect of ebselen bonding to 14-3-3 proteins suggests that disruption of 14-3-3 protein interactions may contribute to the biological effects of ebselen in cancer and neuropsychiatric and infectious disorders. Moreover, ebselen has recently also been proposed as a treatment of COVID-19 and other respiratory viral infections (Sies and Parnham, 2020). Here, we show that ebselen bonding has some specificity and also has differential effects within the highly conserved group of 14-3-3 proteins. However, even more selective binding to specific Cys residues in protein targets may be necessary to achieve the specificity required for further clinical applications of this drug.

Acknowledgments

We greatly appreciate the expert help of Emil Hausvik (University of Bergen) with the fluorescence-based time-dependent protein unfolding experiments and of Anne Baumann (University of Bergen) with the circular dichroism data analysis.

Authorship Contributions

Participated in research design: Hritz, Norton, Martinez, Haavik.

Conducted experiments: Waløen, Jung-KC, Dalla Vecchia, Pandey, Gasparik, Døskeland, Patil, Kleppe.

Performed data analysis: Waløen, Jung-KC, Dalla Vecchia, Gasparik, Døskeland, Patil, Kleppe, Martinez.

Wrote or contributed to the writing of the manuscript: Waløen, Martinez, Haavik.

References

Aitken A (2006) 14-3-3 proteins: a historic overview. *Semin Cancer Biol* **16**:162–172.
Aubi O, Flydal MI, Zheng H, Skjærven L, Rekand I, Leiros HK, Haug BE, Cianciotto NP, Martinez A, and Underhaug J (2015) Discovery of a specific inhibitor of pyomelanin synthesis in Legionella pneumophila. *J Med Chem* **58**:8402–8412.
Azad GK and Tomar RS (2014) Ebselen, a promising antioxidant drug: mechanisms of action and targets of biological pathways. *Mol Biol Rep* **41**:4865–4879.
Ballone A, Centorrino F, and Ottmann C (2018) 14-3-3: a case study in PPI modulation. *Molecules* **23**:1386.
Bier D, Bartel M, Sies K, Halbach S, Higuchi Y, Haranosono Y, Brummer T, Kato N, and Ottmann C (2016) Small-molecule stabilization of the 14-3-3/Gab2 protein-protein interaction (PPI) interface. *ChemMedChem* **11**:911–918.
Böhm G, Muhr R, and Jaenicke R (1992) Quantitative analysis of protein far UV circular dichroism spectra by neural networks. *Protein Eng* **5**:191–195.
Cao L, Lei H, Chang MZ, Liu ZQ, and Bie XH (2015) Down-regulation of 14-3-3β exerts anti-cancer effects through inducing ER stress in human glioma U87 cells: Involvement of CHOP-Wnt pathway. *Biochem Biophys Res Commun* **462**:389–395.
Capper MJ, Wright GSA, Barbieri L, Luchinat E, Mercatelli E, McAlary L, Yerbury JJ, O'Neill PM, Antonyuk SV, Banci L, et al. (2018) The cysteine-reactive small molecule ebselen facilitates effective SOD1 maturation. *Nat Commun* **9**:1693.
Carreño Gutiérrez H, Colanesi S, Cooper B, Reichmann F, Young AMJ, Kelsh RN, and Norton WHJ (2019) Endothelin neurotransmitter signalling controls zebrafish social behaviour. *Sci Rep* **9**:3040.
Chen DY, Dai DF, Hua Y, and Qi WQ (2015) p53 suppresses 14-3-3γ by stimulating proteasome-mediated 14-3-3γ protein degradation. *Int J Oncol* **46**:818–824.
Cornell B and Toyo-Oka K (2017) 14-3-3 proteins in brain development: neurogenesis, neuronal migration and neuromorphogenesis. *Front Mol Neurosci* **10**:318.
Dalla Vecchia E, Di Donato V, Young AMJ, Del Bene F, and Norton WHJ (2019) Reelin Signaling Controls the Preference for Social Novelty in Zebrafish. *Front Behav Neurosci.* Sep 19; **13**:214. doi: 10.3389/fnbeh.2019.00214. eCollection 2019. PMID: 31607872.
Del Campo N, Chamberlain SR, Sahakian BJ, and Robbins TW (2011) The roles of dopamine and noradrenaline in the pathophysiology and treatment of attention-deficit/hyperactivity disorder. *Biol Psychiatry* **69**:e145–e157.
Diallo K, Oppong AK, and Lim GE (2019) Can 14-3-3 proteins serve as therapeutic targets for the treatment of metabolic diseases? *Pharmacol Res* **139**:199–206.
Egan RJ, Bergner CL, Hart PC, Cachat JM, Canavello PR, Elegante MF, Elkhayat SI, Bartels BK, Tien AK, Tien DH, et al. (2009) Understanding behavioral and physiological phenotypes of stress and anxiety in zebrafish. *Behav Brain Res* **205**:38–44.
Favrot L, Grzegorzewicz AE, Lajiness DH, Marvin RK, Boucau J, Isailovic D, Jackson M, and Ronning DR (2013) Mechanism of inhibition of Mycobacterium tuberculosis antigen 85 by ebselen. *Nat Commun* **4**:2748.
Ghorbani S, Fossbakk A, Jorge-Finnigan A, Flydal MI, Haavik J, and Kleppe R (2016) Regulation of tyrosine hydroxylase is preserved across different homo- and heterodimeric 14-3-3 proteins. *Amino Acids* **48**:1221–1229.
Ghosh A, Ratha BN, Gayen N, Mroue KH, Kar RK, Mandal AK, and Bhunia A (2015) Biophysical characterization of essential phosphorylation at the flexible C-terminal region of C-Raf with 14-3-3ζ protein. *PLoS One* **10**:e0135976.
Ghorbani S, Szigetvari PD, Haavik J, and Kleppe R (2020) Serine 19 phosphorylation and 14-3-3 binding regulate phosphorylation and dephosphorylation of tyrosine hydroxylase on serine 31 and serine 40. *J. Neurochem* **152**(1):29–47. doi: 10.1111/jnc.14872.
Goins CM, Dajnowicz S, Thanna S, Sucheck SJ, Parks JM, and Ronning DR (2017) Exploring covalent allosteric inhibition of antigen 85c from mycobacterium tuberculosis by ebselen derivatives. *ACS Infect Dis* **3**:378–387.
Greco TM, Hodara R, Parastatidis I, Heijnen HF, Dennehy MK, Liebler DC, and Ischiropoulos H (2006) Identification of S-nitrosylation motifs by site-specific mapping of the S-nitrosocysteine proteome in human vascular smooth muscle cells. *Proc Natl Acad Sci USA* **103**:7420–7425.
Helander L, Sharma A, Krokan HE, Plaetzer K, Krammer B, Tortik N, Gederaas OA, Slupphaug G, and Hagen L (2016) Photodynamic treatment with hexyl-aminolevulinate mediates reversible thiol oxidation in core oxidative stress signaling proteins. *Mol Biosyst* **12**:796–805.

Hermeking H (2003) The 14-3-3 cancer connection. *Nat Rev Cancer* **3**:931–943.
Ichimura T, Isobe T, Okuyama T, Yamauchi T, and Fujisawa H (1987) Brain 14-3-3 protein is an activator protein that activates tryptophan 5-monooxygenase and tyrosine 3-monooxygenase in the presence of Ca2+,calmodulin-dependent protein kinase II. *FEBS Lett* **219**:79–82.
Jacobsen KK, Kleppe R, Johansson S, Zayats T, and Haavik J (2015) Epistatic and gene wide effects in YWHA and aromatic amino hydroxylase genes across ADHD and other common neuropsychiatric disorders: Association with YWHAE. *Am J Med Genet B Neuropsychiatr Genet* **168**:423–432.
James SJ, Slikker 3rd W, Melnyk S, New E, Pogribna M, and Jernigan S (2005) Thimerosal neurotoxicity is associated with glutathione depletion: protection with glutathione precursors. *Neurotoxicology* **26**:1–8.
Jandova Z, Trosanova Z, Weisova V, Oostenbrink C, and Hritz J (2018) Free energy calculations on the stability of the 14-3-3ζ protein. *Biochim Biophys Acta Proteins Proteomics* **1866**:442–450.
Jiang H, Yu Y, Liu S, Zhu M, Dong X, Wu J, Zhang Z, Zhang M, and Zhang Y (2019) Proteomic study of a Parkinson's disease model of undifferentiated SH-SY5Y cells induced by a proteasome inhibitor. *Int J Med Sci* **16**:84–92.
Jin Z, Du X, Xu Y, Deng Y, Liu M, Zhao Y, Zhang B, Li X, Zhang L, Peng C, et al. (2020) Structure of M^{pro} from SARS-CoV-2 and discovery of its inhibitors. *Nature* **582**:289–293.
Joice AC, Harris MT, Kahney EW, Dodson HC, Maselli AG, Whitehead DC, and Morris JC (2013) Exploring the mode of action of ebselen in Trypanosoma brucei hexokinase inhibition. *Int J Parasitol Drugs Drug Resist* **3**:154–160.
Kim HS, Ullevig SL, Nguyen HN, Vanegas D, and Asmis R (2014) Redox regulation of 14-3-3ζ controls monocyte migration. *Arterioscler Thromb Vasc Biol* **34**:1514–1521.
Kleppe R, Rosati S, Jorge-Finnigan A, Alvira S, Ghorbani S, Haavik J, Valpuesta JM, Heck AJR, and Martinez A (2014) Phosphorylation dependence and stoichiometry of the complex formed by tyrosine hydroxylase and 14-3-3γ. *Mol Cell Proteomics* **13**:2017–2030.
Lass A, Witting P, Stocker R, and Esterbauer H (1996) Inhibition of copper- and peroxyl radical-induced LDL lipid oxidation by ebselen: antioxidant actions in addition to hydroperoxide-reducing activity. *Biochim Biophys Acta* **1303**:111–118.
Li CF, Fang FM, Lan J, Wang JW, Kung HJ, Chen LT, Chen TJ, Li SH, Wang YH, Tai HC, Yu SC, and Huang HY (2014) AMACR amplification in myxofibrosarcomas: a mechanism of overexpression that promotes cell proliferation with therapeutic relevance. *Clin Cancer Res.* **20**(23):6141–52.
Liao W, Wang S, Han C, and Zhang Y (2005) 14-3-3 proteins regulate glycogen synthase 3beta phosphorylation and inhibit cardiomyocyte hypertrophy. *FEBS J* **272**:1845–1854.
Lieberman OJ, Orr MW, Wang Y, and Lee VT (2014) High-throughput screening using the differential radial capillary action of ligand assay identifies ebselen as an inhibitor of diguanylate cyclases. *ACS Chem Biol* **9**:183–192.
Liu M, Liu X, Ren P, Li J, Chai Y, Zheng SJ, Chen Y, Duan ZP, Li N, and Zhang JY (2014) A cancer-related protein 14-3-3ζ is a potential tumor-associated antigen in immunodiagnosis of hepatocellular carcinoma. *Tumour Biol* **35**:4247–4256.
Masaki C, Sharpley AL, Cooper CM, Godlewska BR, Singh N, Vasudevan SR, Harmer CJ, Churchill GC, Sharp T, Rogers RD, et al. (2016) Effects of the potential lithium-mimetic, ebselen, on impulsivity and emotional processing. *Psychopharmacology (Berl)* **233**:2655–2661.
Menéndez CA, Byléhn F, Perez-Lemus GR, Alvarado W, and de Pablo JJ (2020) Molecular characterization of ebselen binding activity to SARS-CoV-2 main protease. *Sci Adv* **6**:eabd0345.
Mukherjee S, Weiner WS, Schroeder CE, Simpson DS, Hanson AM, Sweeney NL, Marvin RK, Ndjomou J, Kolli R, Isailovic D, et al. (2014) Ebselen inhibits hepatitis C virus NS3 helicase binding to nucleic acid and prevents viral replication. *ACS Chem Biol* **9**:2393–2403.
Nery LR, Eltz NS, Martins L, Guerim LD, Pereira TC, Bogo MR, and Vianna MR (2014) Sustained behavioral effects of lithium exposure during early development in zebrafish: involvement of the Wnt-β-catenin signaling pathway. *Prog Neuropsychopharmacol Biol Psychiatry* **55**:101–108.
Niesen FH, Berglund H, and Vedadi M (2007) The use of differential scanning fluorimetry to detect ligand interactions that promote protein stability. *Nat Protoc* **2**:2212–2221.
Obsil T and Obsilova V (2011) Structural basis of 14-3-3 protein functions. *Semin Cell Dev Biol* **22**:663–672.
Pagan C, Goubran-Botros H, Delorme R, Benabou M, Lemière N, Murray K, Amsellem F, Callebert J, Chaste P, Jamain S, et al. (2017) Disruption of melatonin synthesis is associated with impaired 14-3-3 and miR-451 levels in patients with autism spectrum disorders. *Sci Rep* **7**:2096.
Parran DK, Barker A, and Ehrich M (2005) Effects of thimerosal on NGF signal transduction and cell death in neuroblastoma cells. *Toxicol Sci* **86**:132–140.
Pennington KL, Chan TY, Torres MP, and Andersen JL (2018) The dynamic and stress-adaptive signaling hub of 14-3-3: emerging mechanisms of regulation and context-dependent protein-protein interactions. *Oncogene* **37**:5587–5604.
Pozuelo Rubio M, Geraghty KM, Wong BH, Wood NT, Campbell DG, Morrice N, and Mackintosh C (2004) 14-3-3-affinity purification of over 200 human phosphoproteins reveals new links to regulation of cellular metabolism, proliferation and trafficking. *Biochem J* **379**:395–408.
Ren J, Zhao Y, Fry EE, and Stuart DI (2018) Target identification and mode of action of four chemically divergent drugs against ebolavirus infection. *J Med Chem* **61**:724–733.
Sies H and Parnham MJ (2020) Potential therapeutic use of ebselen for COVID-19 and other respiratory viral infections. *Free Radic Biol Med* **156**:107–112.
Singh N, Halliday AC, Thomas JM, Kuznetsova OV, Baldwin R, Woon EC, Aley PK, Antoniadou I, Sharp T, Vasudevan SR, et al. (2013) A safe lithium mimetic for bipolar disorder. *Nat Commun* **4**:1332.
Singh N, Sharpley AL, Emir UE, Masaki C, Herzallah MM, Gluck MA, Sharp T, Harmer CJ, Vasudevan SR, Cowen PJ, et al. (2016) Effect of the putative lithium mimetic ebselen on brain myo-inositol, sleep, and emotional processing in humans. *Neuropsychopharmacology* **41**:1768–1778.
Skjevik AA, Mileni M, Baumann A, Halskau O, Teigen K, Stevens RC, and Martinez A (2014) The N-terminal sequence of tyrosine hydroxylase is a conformationally versatile motif that binds 14-3-3 proteins and membranes. *J Mol Biol* **426**:150–168.
Stevers LM, Sijbesma E, Botta M, MacKintosh C, Obsil T, Landrieu I, Cau Y, Wilson AJ, Karawajczyk A, Eickhoff J, et al. (2018) Modulators of 14-3-3 protein-protein interactions. *J Med Chem* **61**:3755–3778.
Sugden PH, Fuller SJ, Weiss SC, and Clerk A (2008) Glycogen synthase kinase 3 (GSK3) in the heart: a point of integration in hypertrophic signalling and a therapeutic target? A critical analysis. *Br J Pharmacol* **153** (Suppl 1):S137–S153.
Torrico B, Antón-Galindo E, Fernàndez-Castillo N, Rojo-Francàs E, Ghorbani S, Pineda-Cirera L, Hervás A, Rueda I, Moreno E, Fullerton JM, et al. (2020) Involvement of the 14-3-3 gene family in autism spectrum disorder and schizophrenia: genetics, transcriptomics and functional analyses. *J Clin Med* **9**:1851.
Urbaneja MA, Skjærven L, Aubi O, Underhaug J, López DJ, Arregi I, Alonso-Mariño M, Cuevas A, Rodríguez JA, Martinez A, et al. (2017) Conformational stabilization as a strategy to prevent nucleophosmin mislocalization in leukemia. *Sci Rep* **7**:13959.
Valenti D, Neves JF, Cantrelle FX, Hristeva S, Lentini Santo D, Obšil T, Hanoulle X, Levy LM, Tzalis D, Landrieu I, et al. (2019) Set-up and screening of a fragment library targeting the 14-3-3 protein interface. *MedChemComm* **10**:1796–1802.
van Heusden GPH (2005) 14-3-3 proteins: regulators of numerous eukaryotic proteins. *IUBMB Life* **57**:623–629.
Vaudel M, Burkhart JM, Zahedi RP, Oveland E, Berven FS, Sickmann A, Martens L, and Barsnes H (2015) PeptideShaker enables reanalysis of MS-derived proteomics data sets. *Nat Biotechnol* **33**:22–24.
Vilchez D, Saez I, and Dillin A (2014) The role of protein clearance mechanisms in organismal ageing and age-related diseases. *Nat Commun* **5**:5659.
Waløen K, Kleppe R, Martinez A, and Haavik J (2017) Tyrosine and tryptophan hydroxylases as therapeutic targets in human disease. *Expert Opin Ther Targets* **21**:167–180.
Wang Y, Wallach J, Duane S, Wang Y, Wu J, Wang J, Adejare A, and Ma H (2017) Developing selective histone deacetylases (HDACs) inhibitors through ebselen and analogs. *Drug Des Devel Ther* **11**:1369–1382.
Woodcock JM, Coolen C, Goodwin KL, Baek DJ, Bittman R, Samuel MS, Pitson SM, and Lopez AF (2015) Destabilisation of dimeric 14-3-3 proteins as a novel approach to anti-cancer therapeutics. *Oncotarget* **6**:14522–14536.
Xiao Y, Lin VY, Ke S, Lin GE, Lin FT, and Lin WC (2014) 14-3-3τ promotes breast cancer invasion and metastasis by inhibiting RhoGDIα. *Mol Cell Biol* **34**:2635–2649.
Yang X, Lee WH, Sobott F, Papagrigoriou E, Robinson CV, Grossmann JG, Sundström M, Doyle DA, and Elkins JM (2006) Structural basis for protein-protein interactions in the 14-3-3 protein family. *Proc Natl Acad Sci USA* **103**:17237–17242.

Address correspondence to: Jan Haavik, Department of Biomedicine, University of Bergen, 5009 Bergen, Norway. E-mail: jan.haavik@uib.no; or Aurora Martinez, Department of Biomedicine, University of Bergen, 5009 Bergen, Norway. E-mail: aurora.martinez@uib.no

Supplemental data for manuscript # MOLPHARM-AR-2020-000184

Cysteine modification by ebselen reduces the stability and cellular levels of 14-3-3 proteins

Kai Waløen, Jung K.C. Kunwar, Elisa D. Vecchia, Sunil Pandey, Norbert Gasparik, Anne Døskeland, Sudarshan Patil, Rune Kleppe, Jozef Hritz, William H.J. Norton, Aurora Martinez, and Jan Haavik

ID	Drug name	Formula	Therapeutic class/ therapeutic effect	ΔT_m at 400 µM (◦C)
1	Fulvestrant*	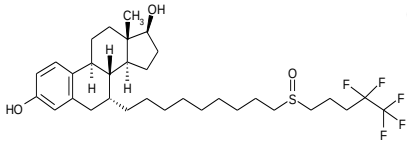	Endocrinology/ Antineoplastic	-23.6
2	Cefoxitin	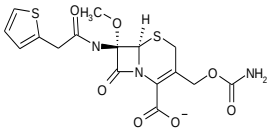	Metabolism/ Antibacterial	-17.3
3	Thimerosal	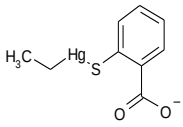	Infectiology/ Antiseptic	-11.7
4	Rabeprazole[1]	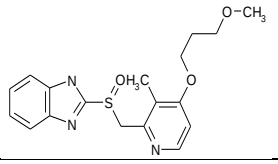	Metabolism/ Antiulcer	-11.4
5	Mercaptopurine	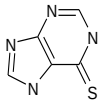	Immunology/ Immunosuppressant	-10.8
6	Thioguanosine	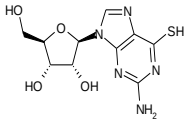	Metabolism/ Antineoplastic	-9.2
7	Tenatoprazole[1]	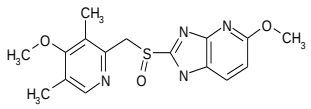	Metabolism/ Antiulcer	-8.6
8	Altrenogest*	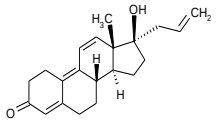	Endocrinology/ Progestogen	-8.4
9	Nifedipine[2]	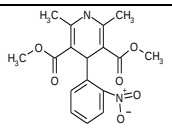	Cardiovascular/ Antianginal	-7.2
10	Pinaverium[2]	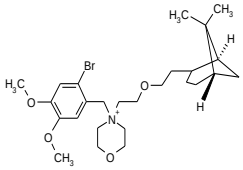	Neuromuscular/ Antispastic	-6.7
11	Ebselen	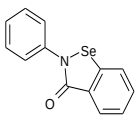	Metabolism/ Anti-inflammatory	-7.0

12	Lansoprazole[1]	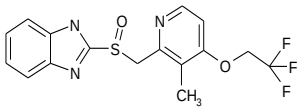	Metabolism/ Antiulcer	-6.0
13	Cefaclor	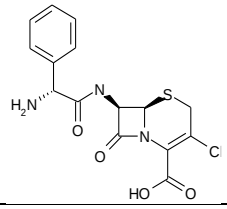	Infectiology/ Antibacterial	-6.0
14	Nisoldipine[2]	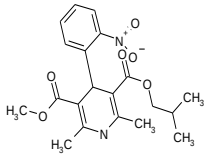	Cardiovascular/ Antianginal	-5.8
15	Carbenoxolone*,[3]	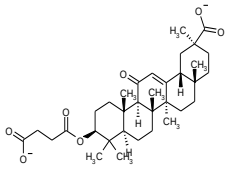	Metabolism/ Antiulcer	-5.1

Supplemental Table 1. Small-molecule drug hits obtained from the primary DSF screen. The midpoint melting temperature (T_m) of 14-3-3ζ with 4% DMSO was 61.1 ± 0.5°C, and 15 hits that caused $|\Delta T_m| \geq 10$ x SD (5.1°C), used as a cut-off value, were selected for concentration dependent studies. Based on its consistent concentration-dependent effect and reduced toxicity, ebselen was selected for further studies. *Steroids. [1]Proton pump inhibitor. [2]Calcium channel blocker [3]Probable calcium channel blocker

Supplemental Figure S1. Amino acid sequences of the seven isoforms of 14-3-3 are presented. The cysteine residues are highlighted in yellow.

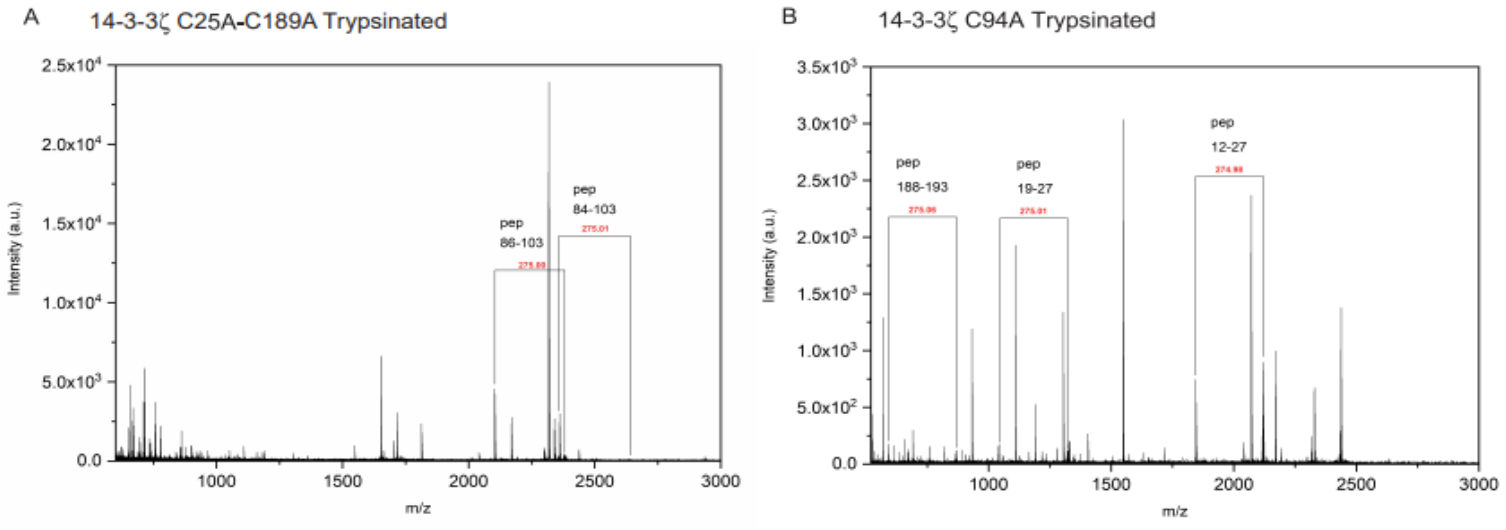

Supplemental Figure S2. MALDI-TOF MS/MS peptide analysis of trypsin digested 1433ζ mutant constructs. a) 1433ζ-C25A-C189A and b) 1433ζ-C94A, after ebselen treatment. Peptides containing cysteines in tagged and untagged form (peptides with a mass shift of 275 Da) are denoted. In a) the figure shows two peptides involving ebselen tagging of C94 in very small amounts. In b) the figure shows a peptide involving C189 and two peptides involving C25.

Supplementary Figure S3. Viability of SHSY5Y cells treated with increasing concentration of ebselen and ebselen oxide. A Cell Titer-Blue assay was performed to examine cell viability of SHSY5Y cells treated with increasing concentration of ebselen and ebselen oxide. The cells were plated in 96-well plates at the density of 25000 cells per well and 5 h later were treated with different concentration of ebselen, ebselen oxide and DMSO (0.05%). Cells were then incubated for 16 h and then 20 µL of Cell Titre Blue reagent was added to each well. The plates were incubated for 2hrs before the fluorescence (λ=590) was measured with Victor 3 1420 Multilabel counter plate reader. A, Cell images using ebselen, B, relative cell viability using ebselen, C Cell images using ebselen oxide D, relative cell viability with ebselen oxide. Statistical analyses by 2-tailed Student's t test. (*) p< 0.05, (**) p < 0.005, (***) p < 0.001, (****) p < 0.0001. All data are presented as mean ± SEM.

A

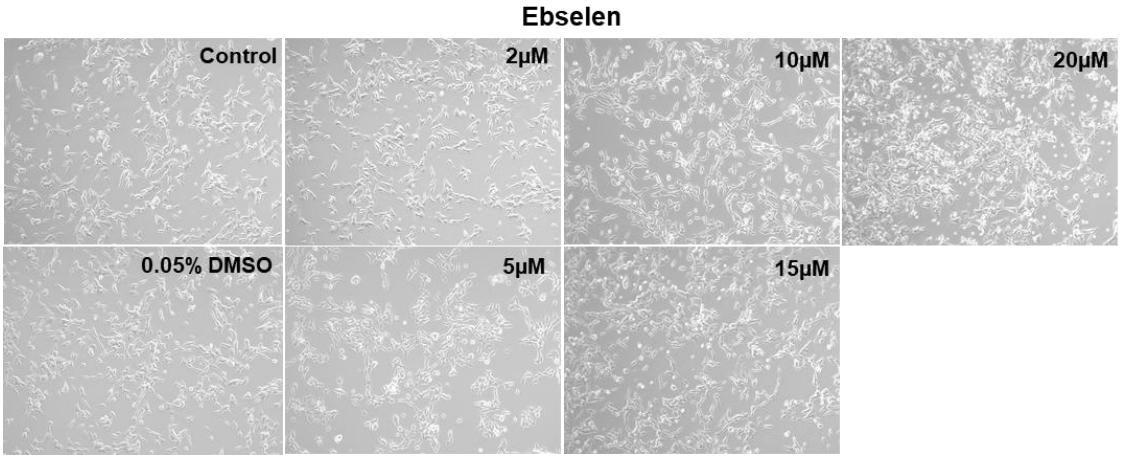

B

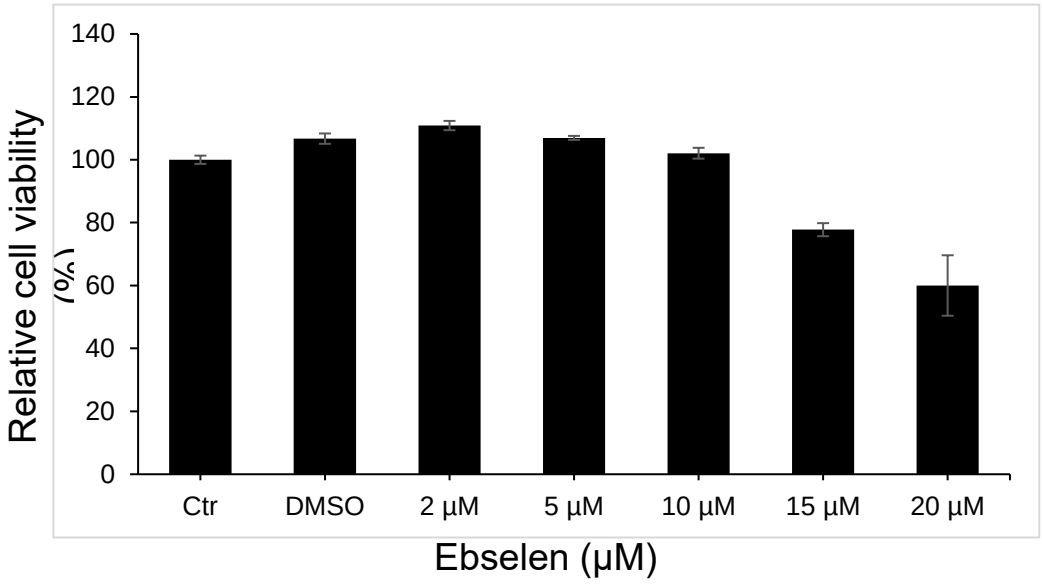

C

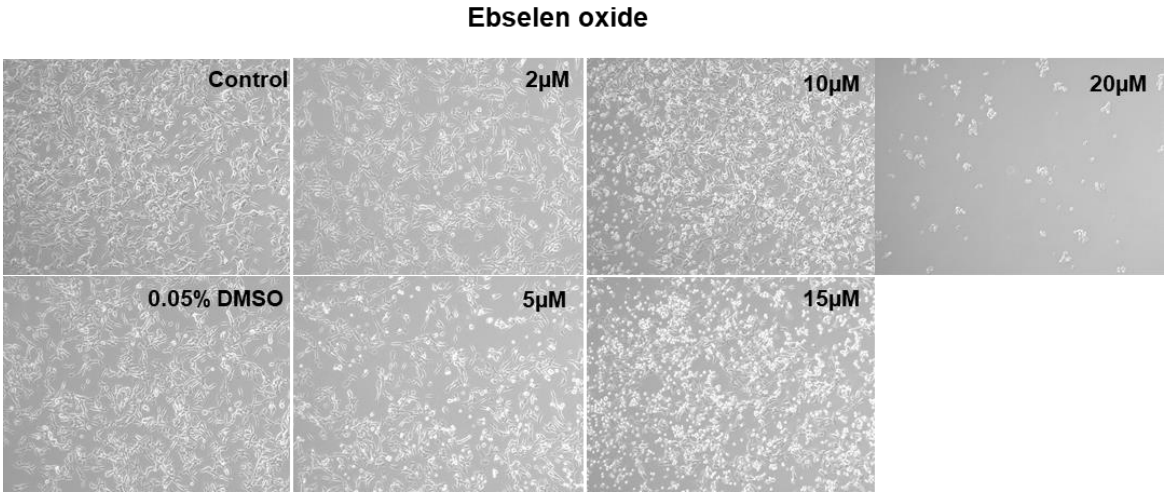
Ebselen oxide
Control
2μM
10μM
20μM
0.05% DMSO
5μM
15μM

D

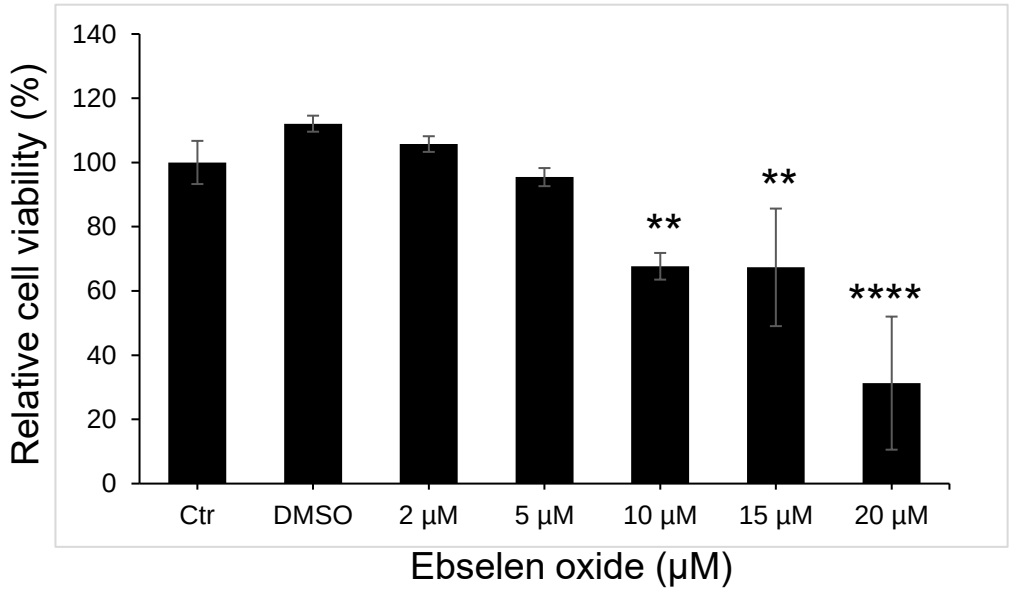
Relative cell viability (%)
140
120
100
80
60
40
20
0
**
**
****
Ctr
DMSO
2 μM
5 μM
10 μM
15 μM
20 μM
Ebselen oxide (μM)